COMPUTATIONAL LASER MICROMACHINING MODEL FOR MACHINING PMMA

TIONG CHUNG SHIA

BACHELOR OF ENGINEERING

UNIVERSITI MALAYSIA PAHANG

2010

COMPUTATIONAL LASER MICROMACHINING FOR MACHINING PMMA

TIONG CHUNG SHIA

Report submitted in partial fulfillment of the requirements for the award of the degree of Bachelor of Mechanical Engineering with Manufacturing Engineering

Faculty of Mechanical Engineering
UNIVERSITI MALAYSIA PAHANG

DECEMBER 2010

UNIVERSITI MALAYSIA PAHANG

FACULTY OF MECHANICAL ENGINEERING

We certify that the project entitled “Computational Laser Micromachining Model for Machining PMMA” is written by Tiong Chung Shia. We have examined the final copy of this project and in our opinion; it is fully adequate in terms of scope and quality for the award of the degree of Bachelor of Engineering. We herewith recommend that it be accepted in partial fulfillment of the requirements for the degree of Bachelor of Mechanical Engineering with Manufacturing Engineering.

Dr. Ahmad Razlan Yusoff

Examiner Signature

SUPERVISOR'S DECLARATION

I hereby declare that I have checked this project and in my opinion, this project is adequate in terms of scope and quality for the award of the degree of Bachelor of Mechanical Engineering with Manufacturing Engineering.

Signature
Name of Supervisor: Dr. Daw Thet Thet Mon
Position: Senior Lecturer
Date: 6th December 2010

STUDENT'S DECLARATION

I hereby declare that the work in this project is my own except for quotations and summaries which have been duly acknowledged. The project has not been accepted for any degree and is not concurrently submitted for award of other degree.

Signature
Name: Tiong Chung Shia
ID Number: ME07032
Date: 6th December 2010

Dedicated to my parents

ACKNOWLEDGEMENTS

I am grateful and would like to express my sincere gratitude to my supervisor Dr. Daw Thet Thet Mon for her germinal ideas, invaluable guidance, continuous encouragement and constant support in making this project possible. I appreciate her consistent support from the first day I applied to graduate program to these concluding moments. I am truly grateful for her progressive vision about my training in science, her tolerance of my naïve mistakes, and her commitment to my future career.

My sincere thanks go to all the members of the staff of the Faculty of Mechanical Engineering, UMP, who helped me in many ways by giving their fully co-operation and commitments. They made my stay at UMP pleasant and unforgettable. Many special thanks go to member laser research group for their excellent co-operation, inspirations and supports during this project.

I acknowledge my sincere indebtedness and gratitude to my parents for their love, dream and sacrifice throughout my life. I acknowledge the sincerity of my sisters who consistently encouraged me to carry on my degree. I cannot find the appropriate words that could properly describe my appreciation for their devotion, support and faith in my ability to attain my goals. Special thanks should be given to my classmates. I would like to acknowledge their supports, comments and suggestions, which was crucial for the successful completion of this study.

ABSTRACT

Laser micromachining has many technological advantages compared to conventional technologies, including design flexibility, production of complex shape and possibility of rapid prototyping. Typical problems that may be faced with laser micromachining are laser-induced debris, large heat-affected zone and laser penetration depth. Frequently, high quality components are obtained by chance or at the expense of time and money due to inaccessible machining dimension, improper set of process parameter and large uncertainty in the process itself. To solve these problems, virtual laser micromachining with the aid of computational model is greatly desirable. This thesis presents a computational laser micromachining model for machining Polymethyl Methacrylate (PMMA). Laser micromachining parameters considered were laser power, spatial velocity and spot size. Finite element models were developed to simulate laser micromachining of PMMA. Time-dependent thermal analysis was used as analysis type. The geometry of the computational model is limited to two-dimensional (2-D) model and uniform mesh design is used. Material was modeled as isotropic and properties were obtained from literature. From result, the computational model was validated by comparing computed size of major cutting zone with experimental result. After validation, laser micromachining was simulated for varying laser parameters generated by design of experiment (DOE) in STATISTICA. These results will be analyzed in STATISTICA and the feasible process parameters were identified. Different parameter combinations provide different contour pattern and different size of major cutting zone. Laser power was found to be the most significant effect to the size of major cutting zone, followed by laser spot size and spatial velocity.

ABSTRAK

Laser mikro-mesin mempunyai banyak keunggulan teknologi berbanding dengan teknologi konvensional, termasuk fleksibiliti rekabentuk, pengeluaran bentuk yang kompleks dan kemungkinan prototyping cepat. Masalah khas yang mungkin dihadapi dengan laser mikro-mesin adalah laser-puing diinduksi, zon terkena panas yang besar dan kedalaman penetrasi laser. Sering, komponen berkualiti tinggi diperolehi secara kebetulan atau dengan mengorbankan masa dan wang kerana dimensi enjin tidak dapat dicapai, set parameter proses yang tidak tepat dan ketidaktentuan yang besar dalam proses itu sendiri. Untuk mengatasi masalah ini, laser mikro-mesin virtual dengan bantuan model pengkomputeran sangat dikehendaki. Tesis ini membentangkan model laser mikro-mesin pengkomputeran untuk mesin Polimetil Metakrilat (PMMA). Parameter laser mikro-mesin yang diambil kira adalah kuasa laser, kelajuan spasial dan saiz spot. Model Finite Elemen telah dibina untuk mensimulasikan laser mikro-mesin untuk PMMA. Analisis terma yang bergantung pada masa digunakan sebagai jenis analisis. Geometri dari model pengkomputeran terhad pada dua dimensi (2-D) model dan reka bentuk mesh seragam digunakan. Bahan dimodelkan sebagai isotropik dan cirri-ciri diperolehi daripada kesusasteraan. Dari keputusan, model pengkomputeran dikenal pastikan dengan membandingkan saiz zon pemotongan utama dengan keputusan eksperimen. Setelah pengesahan, laser mikro-mesin disimulasikan untuk parameter laser yang dihasilkan oleh rekabentuk eksperimen di Statistica. Keputusan ini akan dianalisa di Statistica dan parameter proses yang layak dikenalpasti. Kombinasi parameter yang berbeza memberikan pola kontur yang berbeza dan saiz zon pemotongan utama yang berbeza. Kuasa laser merupakan pengaruh yang paling signifikan terhadap saiz zon pemotongan utama, diikuti dengan saiz laser spot dan kelajuan spasial.

TABLE OF CONTENTS

LIST OF TABLES

LIST OF FIGURES

LIST OF SYMBOLS

A	Area
c	Material specific heat
d	Spot size
d_0	Diameter of the beam at the focusing lens
d_{min}	Theoretical resolution
f	Focal length of the lens
h	Convection coefficient
k	Material thermal conductivity
ρ	Material density
P	Power
q	Heat flux
Q	Internal heat generation rate
s	The size of major cutting zone
T	Temperature of surface of the body
T_a	Ambient fluid temperature
U	Internal energy
V	Spatial velocity
λ	Wavelength of the laser

LIST OF ABBREVIATIONS

Ar	Argon
CAD	Computer-aided design
CAE	Computer-aided engineering
CAM	Computer-aided manufacturing
CO_2	Carbon dioxide
DOE	Design of experiment
DP	Diode-pumped
FE	Finite element
FEA	Finite element analysis
FEM	Finite element method
HAZ	Heat affected zone
IR	Infra-Red
Kr	Krypton
Nd-YAG	Neodymium-Yttrium Aluminium Garnet
PMMA	Polymethyl Methacrylate
UV	Ultraviolet
Xe	Xenon
2-D	Two-dimensional
3-D	Three-dimensional

CHAPTER 1

INTRODUCTION

1.1 PROJECT BACKGROUND

Laser as it is known today has many applications especially in medical sector and in manufacturing sectors. Such application as welding and cutting, measuring or surveying a long distance, laser nuclear fusion, laser treatment and sensing are well-known to name a few (Agrawal and Dutta, 1986). More importantly laser had been used in micromachining since the last decade. The use of laser in micromachining has been a break-through technology since various types of laser were commercially available. Laser micromachining has many technological advantages compared to conventional technologies, including design flexibility, production of complex shape and possibility of rapid prototyping. Indeed, laser micro-fabrication had become one of the fast growing field of science and technology.

Laser micromachining is definitely a good alternative and unique way of processing materials which involve less thermal distortion and minimum metallurgical damage to work piece, compared to conventional methods such as photolithography, etching, LIGA, mechanical micromachining (Pryputniewicz, 2006). Laser involved in micromachining was only involving thermal effect of infrared laser beams to heat, melt and vaporize materials in the early stage. However, with the advance in technology, shorter wavelength ultraviolet (UV) and as well as ultrafast pulsing were discovered, a thermal mechanisms and interactions between beams material can be generated that are shorter than the mean free time between collisions in atoms and molecules. Moreover, micro machining with laser can also be very accurate and neglect the damage from thermal. Application in laser micromachining involve laser bonding of wafer, laser micromachining of three-dimensional (3-D) microchannel system in chemical, biomedical, DNA and environmental science (Pryputniewicz, 2006).

Typical problems that may be faced with laser micromachining are laser-induced debris, large heat affected zone (HAZ) and laser penetration depth. Frequently, high quality components are obtained by chance or at the expense of time and money due to inaccessible machining dimension, improper set of process parameter and large uncertainty in the process itself. To tackle these problems, virtual laser micromachining with the aid of computational model is greatly desirable. Furthermore, now with the development of advanced virtual technology and CAD/CAM/CAE system many realistic designs, analysis and simulations can be done on the computer prior to actual manufacturing.

As for Polymethyl Methacrylate (PMMA), it is a clear plastic, used as a shatterproof replacement for glass. The use of PMMA as the substrate material has several advantages and of it is that PMMA can prevent the contamination caused by biomolecule adsorption since it’s a non-porous solid (Cheng et al., 2004). High clarity in combination with UV-resistance, modest impact strength, and abrasion-resistance make them useful especially in microstructure application such as micro nozzle and micro channels.

In this project, laser micromachining of various parameter combinations were carried out in finite element environment. In order to do so, novel computational models were developed using finite element modeling technique as this technique has been matured enough to develop reliable models (Michael, 2006). The models will help to determine the appropriate process parameters that would produce the high quality surface finish.

1.2 PROBLEM STATEMENT

The problem statements of this project are:

i. Detail experimental study of laser micromachining is expensive.
ii. Feasible laser micromachining parameter for PMMA is not well-known.

1.3 PROJECT OBJECTIVES

The objectives of this project are:

i. To develop a computational model that can simulate laser micromachining of PMMA.
ii. To validate the computational model with experimental result.
iii. To predict the parameter combinations during laser micromachining.

1.4 PROJECT SCOPES

The scopes of this project are:

i. The finite element code ALGOR will be used to develop computational model.
ii. The geometry of the computational model is limited to two-dimensional model.
iii. Isotropic material model will be used for a laser micromachining analysis.
iv. Simulation of laser micromachining will be carried out for various laser power, spatial velocity and spot size using computational model.
v. The computational result will be verified with experimental laser micromachining result done by others.
vi. Laser source used is Neodymium-Yttrium Aluminium Garnet (Nd-YAG) pulse laser.

1.5 OVERVIEW OF THE THESIS

This thesis consists of five chapters. Chapter 1, which is the introduction, states the project background, problem statement, project objectives and project scopes. Chapter 2 is the literature review where study is made on related studies from the previous researchers. Chapter 3 is the methodology of this project that describes the method, procedure and approach that had been used. Chapter 4 is the results and discussion of this project while chapter 5 is the conclusion and recommendation that had been made according to this project.

CHAPTER 2

LITERATURE REVIEW

2.1 INTRODUCTION

The main purpose of this chapter is to collect all the information related to this project with references from various sources such as books, journals, thesis and internet. A review of the literature was performed to identify studies that relevant to this project.

2.2 LASER MICROMACHINING

Laser micromachining is a direct machining method and is based on the interaction of laser light with solid matter. It uses intense ultraviolet (UV) or infrared radiation that provided by a laser to remove the polymer material. The removal mechanism is affected by the radiation wavelength used. Ultraviolet lasers in wavelengths of 157 to 351 nm are mostly used on polymers. If infrared lasers are used, the irradiated material is heated and decomposes, leaving a void in the polymer material. If UV radiation is used, the irradiated polymer decomposes, presumably by a mixture of two mechanisms: thermal and direct bond breaking, Thermal bond breaking is induced by heat, as with infrared radiation. In direct bond breaking, polymer molecules directly absorb ultraviolet photons, often absorbing enough energy so that the chemical bonds within the polymer chains are broken. The resulting smaller polymer chains are volatile or melt at much lower temperatures than the bulk polymers, thereby leaving a void in the material (Geschke et al., 2004).

Laser micromachining includes a wide range of processes where material is removed accurately but the term is also used to describe processes such as microjoining and microadjustment by laser beam. Most applications are found in the electronics industry in high-volume production. Lasers used for micromachining are characterized by short pulse lengths from the millisecond range for applications like mocrowelding to the pico- and even femtosecond area for ablation of metals (McGeough, 2002).

2.3 POLYMETHYL METHACRYLATE

In this project, Polymethyl Methacrylate (PMMA) is selected as the material as it is widely used recently. Figure 2.1 shows an example of PMMA.

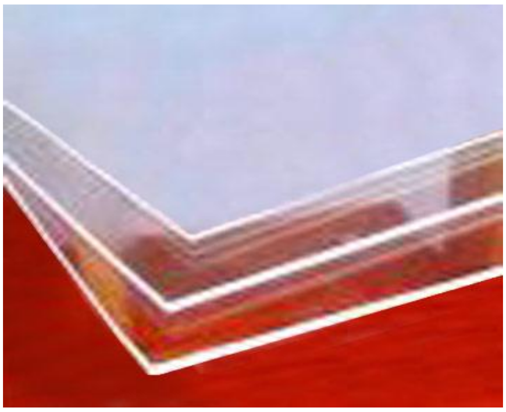

Figure 2.1: Polymethyl Methacrylate

PMMA is a versatile thermoplastic that is well suited for engineering and many common applications. PMMA is usually referred to as its commercial name which is acrylic. PMMA is used frequently in laser machining research as a material to prove the concept due to its low melting temperature, low sensible and latent heat and evaporation nature in phase change. Besides, it is one of the most suitable thermoplastic polymers for machining due to its thermal stability, chemical resistances, and low cost (ETHZ, 2006). PMMA also finds a wide range of applications in automotive, medical, industrial and consumer areas because of its excellent optical property and good weatherability, which is defined as the resistance to the detrimental effects under exposure to the environment.

Unmodified PMMA is almost completely transparent as glass and is utilized as a substitute for glass due to its inexpensive, nonpoisonous, weatherproof, lightweight, burns without residue and unbreakable nature. These favorable properties make it interesting for many uses. Typical automotive applications for PMMA include signal light devices for traffic, nameplates, display panels and glazing. Industrial applications for PMMA include display shelving, signs, instrument panel covers, lenses and skylighting (Liu, 1996).

The effects of CO_2 cutting parameters on the resulting cut quality for polymers were investigated by several researchers. Caiazzo et al. (2005) presented the application of the CO_2 laser cutting process to three thermoplastic polymers in different thicknesses ranging from 2 to 10 mm. They examined laser power, cutting speed, gas pressure, and thickness as cutting parameters. Davim et al. (2008) investigated cutting quality of PMMA by using CO_2 lasers. They presented some surface quality aspects of CO_2 laser cutting of linear and complex 2D. The effect of the process parameters (laser power and cutting velocity) on the quality of the cut for several polymeric materials was also investigated by Davim et al. (2008).

2.4 LASER TYPES

There are different types of lasers. Lasers can be divided into groups according to the different criteria:

i. The state of matter of the active medium: solid, liquid, gas, or plasma.
ii. The spectral range of the laser wavelength: visible spectrum, Infra-Red (IR) spectrum, etc.
iii. The excitation (pumping) method of the active medium: Optic pumping, electric pumping, etc.
iv. The characteristics of the radiation emitted from the laser.
v. The number of energy levels which participate in the lasing process.

These lasers are described as follows:

2.4.1 Gas lasers

Gas lasers can be categorized into the following three sub-groups according to the composition of the lasing medium: neutral atom, ion and molecular. For neutral atom laser, the active medium in these lasers is a noble gas in its neutral state, or a metal power. The helium–neon laser is a typical neutral atom laser and is used widely for applications of measurement, holography, alignment and vision. The laser active medium for ion gas lasers is composed of ionized gas. Ion gas lasers such as argon (Ar), krypton (Kr), and xenon (Xe) are used in applications such as surgery and spectroscopy. Molecular gas laser is where the laser active medium is composed of gas molecules. The most commonly used molecular laser is the carbon dioxide (CO_2) laser although carbon monoxide laser is also being used. A far infrared electromagnetic radiation with 10.6µm wavelength is emitted from a carbon dioxide laser. The lasing medium is a combination of the gases carbon dioxide, helium and nitrogen with the mixture ratio of roughly 5 %, 80 % and 15 % (Liu, 1996).

In particular, carbon dioxide laser ablation is considered as the most attractive and effective method for the polymer-based microfluidic device fabrication due to its inexpensive price and flexibility. Klank et al. (2002) first reported the CO_2 laser micromachining and back-end processing for the rapid production of PMMA based microfluidic systems. Furthermore, Jensen et al. (2003) used a CO_2 laser to produce cavities and microstructures in PMMA by moving the laser beam over the PMMA surface in a raster pattern. Huang et al. (2009) carried out their experiment using a commercially available CO_2 laser machine (F1-50W, HM Laser Machinery Co., LTD., China) which has a wavelength of 10.6 mm and a maximum output power of 50 W in the continuous-wave operation mode to cut the PMMA sheets.

2.4.2 Solid state lasers

The active medium in solid state lasers is a crystal or glass. Solid state lasers use ions in a crystalline matrix to produce laser light. The ions provide the electrons for excitation and the crystalline matrix propagates the energy between ions. Solid state lasers emit radiation in either pulsed mode or in continuous mode. Neodymium-Yttrium

Aluminium Garnet (Nd-YAG) laser is by far the most commonly used solid-state laser. Figure 2.2 shows diode-pumped continuous wave (CW) Nd-YAG laser.

Figure 2.2: Diode-pumped CW Nd-YAG laser

Nd-YAG lasers has laser output in the near infrared region with 1.06 µm wavelength. Although the YAG crystal has a relatively high thermal conductivity, continuous wave operation is limited to cutting since the achievable power is not very high due to the cooling problem of the heated YAG crystal. Nd-YAG lasers are generally used in the pulsed operation for scribing and marking due to the achievable high power and high pulsing rates. Solid state lasers use krypton, xenon, or semi-conductor laser diodes for optical pumping. Krypton flash lamps are useful for continuous wave operation while xenon flash lamps are used for pulsed mode operation since they can support the high current density required in pulsing. (Liu, 1996) The others solid state lasers include Ruby Laser, Neodymium (Nd) laser, Alexandrite Laser, Color Center Laser and Titanium Sapphire Laser (Arieli, undated).

In this project, laser micromachining of PMMA sheet is done by using Nd-YAG laser. Experimental results published in literature show that the Nd:YAG laser has some unique characteristics. Although the mean beam power is relatively low, the beam intensity can be relatively high due to smaller pulse duration and better focusing behaviour. Smaller kerf width, micro-size holes, narrower heat affected zone (HAZ) and better cut edge kerf profile can be obtained in Nd:YAG laser beam machining. Due to shorter wavelength, Nd:YAG laser is highly absorbed when falling even on a reflective surface (Dubey and Yadava, 2008).

The enhanced transmission through plasma, wider choice of optical materials and flexibility in handling with the advent of fibre optic beam delivery are also interesting characteristics of the Nd:YAG laser (Norikazu et al., 1996). Thick materials can be cut in pulsed mode operation which offers high peak power. The development of short pulse lasers using diode-pumped (DP) and Q-switching techniques (for frequency doubling and tripling) enables Nd:YAG lasers to be very useful tool in the field of micromachining (Meijer, 2004). In recent years, pulsed Nd:YAG lasers are being applied for precision cutting of thin sheets with narrow kerf, micro-drilling of holes and intricate profile cut.

2.4.3 Liquid lasers

Liquid lasers are mainly dye lasers using large organic dye molecules as the lasing medium. These dyes are capable of absorbing radiation from a wide range of frequencies in the spectrum from which the lasing can occur. The lasers are tunable in the sense that they can lase in the visible spectrum and parts of the infrared and ultra-violet spectra. Therefore, they are desirable for spectroscopic and photochemical applications (Liu, 1996).

Table 2.1 is listed common lasers with their wavelengths.

Table 2.1: Common lasers and their wavelengths

Laser type	Wavelength (nanometers)
Argon Fluoride	193
Xenon Chloride	308 and 459
Xenon Fluoride	353 and 459
Helium Cadmium	325 - 442
Rhodamine 6G	450 - 650

Source: Aldrich (undated)

Table 2.1: Continued

Laser type	Wavelength (nanometers)
Copper Vapor	511 and 578
Argon	457 - 528 (514.5 and 488 most used)
Frequency doubled Nd:YAG	532
Helium Neon	543, 594, 612, and 632.8
Krypton	337.5 - 799.3 (647.1 - 676.4 most used)
Ruby	694.3
Laser Diodes	630 - 950
Ti:Sapphire	690 - 960
Alexandrite	720 - 780
Nd:YAG	1064
Hydgrogen Fluoride	2600 - 3000
Erbium:Glass	1540
Carbon Monoxide	5000 - 6000
Carbon Dioxide	10600

2.5 LASER MICROMACHINING MECHANISM

Laser is one form of electromagnetic radiation. When the electromagnetic radiation is impinged upon a material surface, some radiation is reflected, some is absorbed and some transmitted. The absoptivity depends on the material, the surface structure, the power density, and the wavelength. With a CO_2 laser about 20 % is absorbed with laser micromachining while with shorter wavelengths such as Nd:YAG 40 to 80 % is absorbed. The remaining part is reflected. Absorption is occurs in a very thin surface layer, where the optical energy is converted into heat (McGeough, 2002).

The material removal mechanism for laser micromachining is a thermal process in which the thermal energy provided by a laser source vaporizes and/or melts the volume of the material to be removed. This thermal natural of material removal provides laser micromachining as a visible alternative for processing difficult-to-machine materials such as ceramics, polymers and composites (Liu, 1996). In plastics, however, the process is quite different. The material is removed by breaking the chemical bonds of the macromolecules, and is dispersed as gas or small particles. No melt is found (McGeough, 2002). Polymers have a relatively low melting point to allow the use of primary forming processes since the material can be easily heated up into a liquid state. In some circumstances, secondary finishing operations are required to achieve the designated dimensional accuracy and the surface quality for polymers (Liu, 1996). In this study, PMMA is to be examined through laser micromachining.

The mechanism of laser beam interaction and material removal is shown in figure 2.3. Firstly, the laser energy is focused on the material surface and partly absorbed. The absorbed energy diffuses into the bulk material by conduction. The high vaporization rate causes a shock wave and a high vapor pressure at the liquid surface considerably increases the boiling temperature. Finally the material is removed as a vapor by the expulsion of melt, as result of the high pressure and by an explosive like boiling of the superheated liquid after the end of the laser pulse.

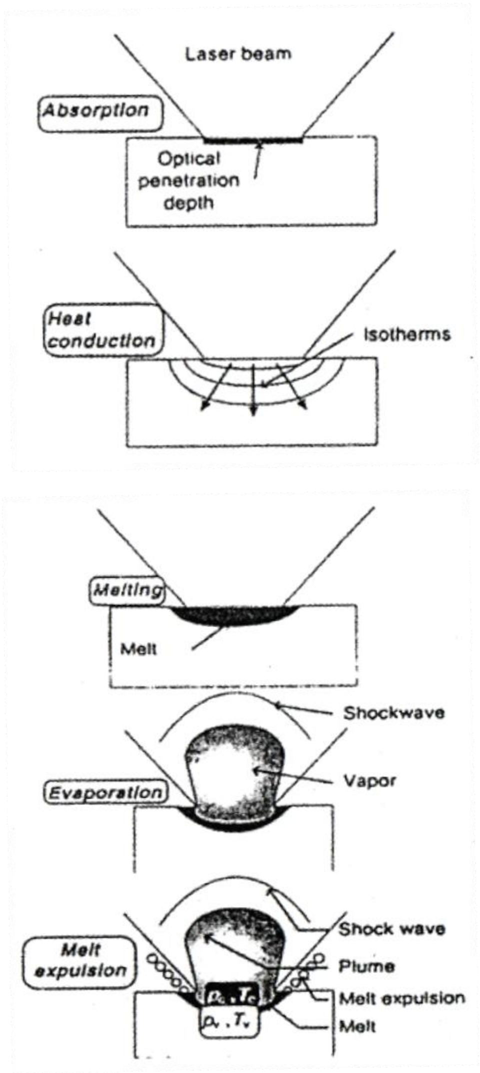

Figure 2.3: Laser micromachining mechanism (McGeough, 2002)

2.6 LASER PROCESSING PARAMETERS

Laser processing parameters have been proven to have a major role on the quality features. In any manufacturing process, it is always desired to know the effect of variation of input parameters on process performance in order to achieve the goal of better product quality. The principal system parameters that affect process quality include the beam power and power density at the focal point, wavelength and focusing system, beam mode, beam form which is continuous wave or pulsed, and beam quality. Some parameters such as beam polarization, assist and/or shielding gas, focal point location, traverse speed, and so on are more process specific (Elijah, 2009).

The major parameter of laser micromachining is the power. The choice of power depends on the desired structure size and the ablation rate. For micromachining purposes, the resolution is limited by the spot size. The theoretical resolution d_{min} (mm) is expressed as in Eq. 2.1,

$$d_{min} = \frac{\lambda f}{\pi d_0} \tag{2.1}$$

Where λ is the wavelength of the laser, d_0 is the diameter of the beam at the focusing lens and f is the focal length of the lens. Thus, the main way of increasing the resolution is by reducing the wavelength (Abgrall and Nguyen, 2009).

Laser micromachining being a non-conventional machining process requires high investment and offers poor efficiency (below 1 %). So, high attention is required for better utilization of resources. The values of process parameters are determined to yield the desired product quality and also to maximize the process performance. There are many factors (variables) such as beam parameters, material parameters and machining parameters which affect the various quality characteristics such as surface roughness, HAZ, and recast layer.

A lot of theoretical and experimental studies have been done by researchers in order to develop the models that try to simulate the conditions during Nd:YAG and laser micromachining to establish the cause and effect relationships between various factors and quality characteristics (Dubey and Yadava, 2008). Zhou and Mahdavian (2004) reported the capability of low power laser to perform tasks other than marking. A theoretical model was developed to estimate the depth of cut with the cutting velocity and laser power for several materials. The agreement between theoretical and experimental results was investigated for a different range of materials. Davim et al. (2008) presented a study to evaluate the effect of the processing parameters (laser power and cutting velocity) under the quality of the cut for several polymeric materials. The parameters used for evaluation of the workability were the dimension of HAZ and the presence and dimension of burr.

2.7 FINITE ELEMENT ANALYSIS

Computer-aided engineering (CAE) is the application of computer software in engineering to evaluate components and assemblies, It encompasses simulation, validation, and optimization of products and manufacturing tools. The primary application of CAE, used in civil, mechanical, aerospace, and electronic engineering, takes the form of finite element analysis (FEA) alongside computer-aided design (CAD).

The finite element method (FEM), sometimes referred to as finite element analysis (FEA), is a computational technique used to obtain approximate solutions of boundary value problems in engineering. Simply stated, a boundary value problem is a mathematical problem in which one or more dependent variable must satisfy a differential equation everywhere within a known domain of independent variables and satisfy specific conditions on the boundary of the domain. Boundary value problems are also sometimes called field problems. The field is the domain of interest and most often represents a physical structure. The field variables are the dependent variables of interest governed by the differential equation. The boundary conditions are the specified values of the field variables on the boundaries of the field. Depending on the type of physical problem being analyzed, the field variables may include physical displacement, temperature, heat flux, and fluid velocity to name only few (Hutton, 2004).

2.7.1 Finite element software

Finite element (FE) package features a flexible model setup, application interfaces and computer-aided design (CAD) import to conduct realistic computer simulation. Finite element software provides a range of simulation tools to help designers and engineers make decisions earlier in the design process. There is a list of software packages that implement the finite element method for solving partial differential equations or aid in the preprocessing and postprocessing of finite element models. The commercial software includes:

i. ALGOR simulation software

   ALGOR simulation software support for multi-CAD environments and extensive finite element modeling tools help manufactures study initial design intent and accurately predict product performance.

ii. NEi Nastran Finite Element Analysis software

   NEi Nastran is a powerful, professional level, finite element analysis tool relied on by major industry groups to simulate and analyze linear and nonlinear stress, dynamics, and heat transfer characteristics of structures and mechanical components.

iii. AxisVM Finite Element Analysis and Design 3D CAD software

   AxisVM is a high-quality software package. Users can build the 3D model with the aid of integrated visual modeling and simple manageability.

iv. Strand7 Full-Featured Finite Element Analysis Software for Windows

   Strand7’s fully-integrated visual environment combined with a suite of powerful solvers gives an unparalleled functionality in a single application. Construct model, run analyses and investigate results simultaneously using a seamless interface. (Azojomo, 2010)

2.7.2 General procedure for finite element analysis

For all analyses whether structural, heat transfer, fluid flow, or some other problem, certain steps in formulating a finite element analysis of a physical problem are common. These steps are embodied in commercial finite element software packages and are described as follows (Hutton, 2004).

i. Preprocessing

The preprocessing step is, quite generally, described as defining the model and includes

- Define the geometric domain of the problem.
- Define the element type(s) to be used.
- Define the material properties of the elements.
- Define the geometric properties of the elements (length, area, and the like).
- Define the element connectivities (mesh the model).
- Define the physical constraints (boundary conditions).
- Define the loadings

The preprocessing (model definition) step is critical. A perfectly computed finite element solution is of absolutely no value if it corresponds to the wrong problem.

ii. Solution

The solution step is described as analyzing the model and includes

- Assemble the element stiffness matrix
- Solve the system of equations
- Calculate the results

iii. Postprocessing

Analysis and evaluation of the solution results is referred to as postprocessing. The result evaluation includes

- Review the results
- Generate a report of the result

2.7.3 Application of finite element method

A variety of specializations under the umbrella of the mechanical engineering discipline commonly use integrated finite element method (FEM) design and development of their products. FEM software provides a wide range of simulation options for controlling the complexity of both modeling and analysis of a system.

Similarity, the desired level of accuracy required and associated computational time requirements can be managed simultaneously to address most engineering applications.

FEM allows entire designs to be constructed, refined, and optimized before the design is manufactured. This powerful design tool has significantly improved both the standard of engineering designs and the methodology of the design process in many industrial applications. The introduction of FEM has substantially decreased the time to take products from concept to the production line. It is primarily through improved initial prototype designs using FEM that testing and development have been accelerated. In summary, benefits of FEM include increased accuracy, enhanced design and better insight into critical design parameters, virtual prototyping, fewer hardware prototypes, a faster and less expensive design cycle, increased productivity, and increased revenue.

2.8 PREVIOUS RESEARCHER'S STUDY RELATED TO THE PROJECT

Previously, Kim and Zhang (2001) have studied a computational model for simulation of pulsed laser-cutting process which has been developed using a finite element method. An unsteady heat transfer model is considered that deals with the material-cutting process using a Gaussian wave laser beam in a pulsed mode. The convergence study with mesh refinements and time steps first identifies optimal mesh and time step for the present analyses. Numerical analyses are carried out on the amount of material removal and groove smoothness with laser power and number of pulses while other laser cutting parameter are fixed. The results show that there exist threshold values in number of pulses and laser power in order to achieve two predetermined conditions: (1) amount of material removal and (2) smoothness of groove shape. These values form an envelope called threshold curve that separate the acceptable region from unacceptable one for quality pulsed laser cutting. The effect of velocity also leads to another threshold curve which is determined from both number of pulses and velocity.

Yang et al. (2010) had conducted an experimental study to characterize the heat affected zone produced when laser heating a Ti6Al4V alloy plate workpiece. The emissivity and absorptivity of the Ti6Al4V alloy were determined experimentally. A 3D transient finite element method for a moving Gaussian laser heat source was developed to predict the depth and width of the heat affected zone on the Ti6Al4V alloy workpiece. There was a close correlation between the experimental data and the simulation results. It was found that the depth and width of the heat affected zone were strongly dependent on the laser parameters (laser power, laser scan speed, the angle of incidence and the diameter of the laser spot) and material properties (thermal conductivity, specific heat and density). Parametric studies showed that the depth and width of the heat affected zone increased with an increase in the laser power and decreased with an increase of the laser spot size and the laser scan speed. The thermal model can be used to determine the laser parameters for a given cut geometry that will yield no residual heat affected zone in the material after cutting. This provides the basis to optimize and improve laser assisted machining technique.

The first aim of the study which done by Chen et al. (2009) was to establish the temperature model of the eggshell by the finite element analysis software ANSYS and realize the eggshell temperature field based on the laser marking processing. The eggshell surface which created the meshing model, set the parameters with the ANSYS Parameter Design Language and simulated that the Gaussian distributed laser beam acted on the surface were established. In addition, marking characters made use of the CO_2 laser processing system on the brittle eggshell to analyze whether laser beams caused damage to the inner of the eggshell. According to the results of the comparison between the simulation by ANSYS and the experiment of laser marking, it is revealed that the heat-affected area by laser marking is similar to that of the simulation.

CHAPTER 3

METHODOLOGY

3.1 INTRODUCTION

This chapter will describe about how the project had been done and the method used to achieve the project objectives. A systematic planning before start a project is very important to make sure the fluent of the project. Therefore, methodology is an important element to provide the guidelines and procedures to ensure this project can be done successfully.

3.2 FLOW CHART

Figure 3.1 shows the process flow in conducting this project:

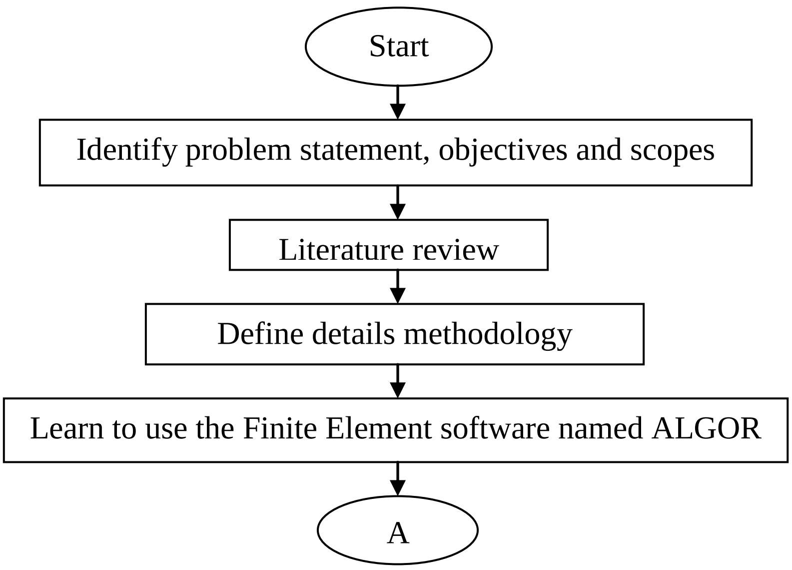

Figure 3.1: Flow Chart for overall Final Year Project

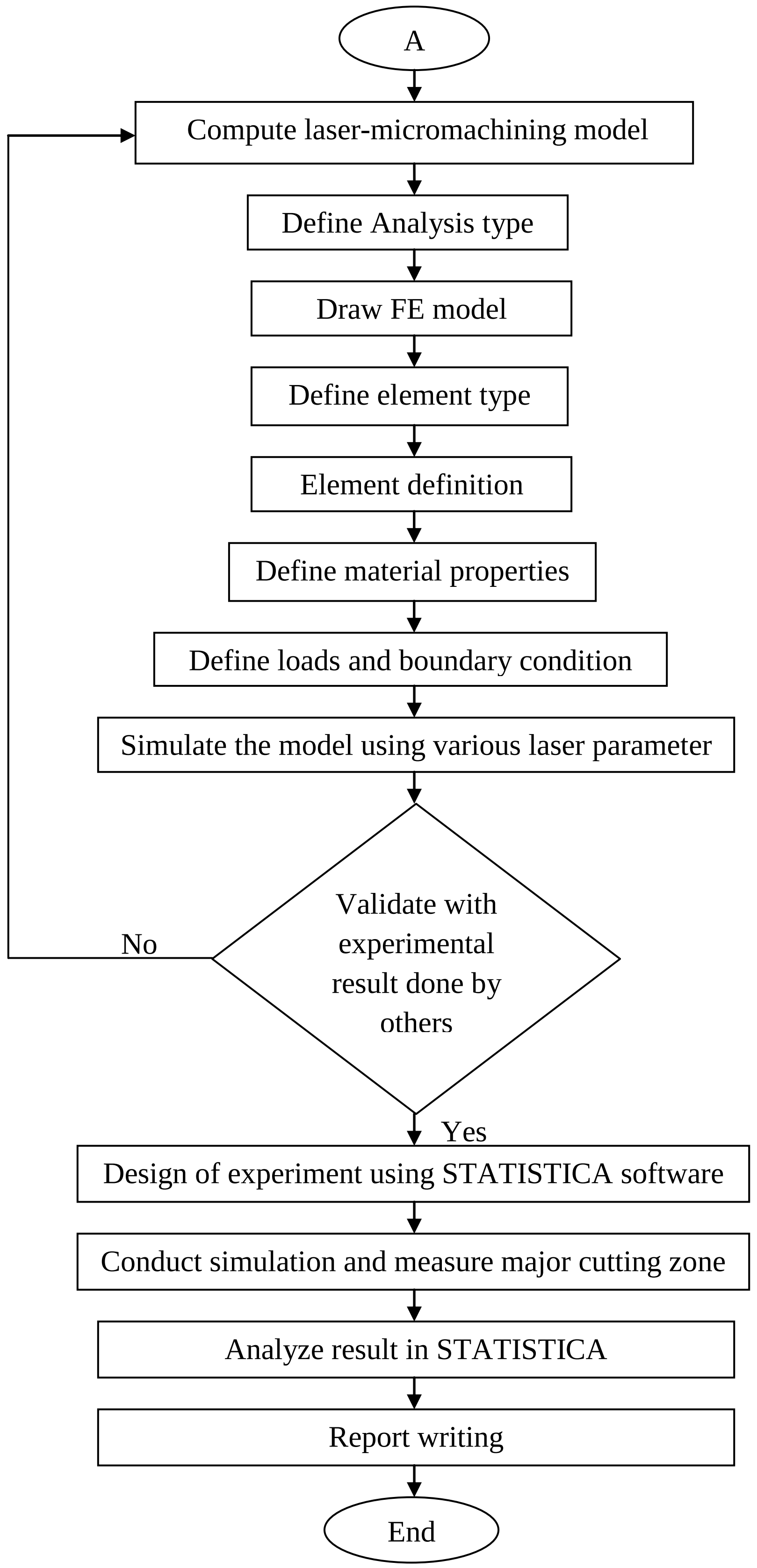

Figure 3.1: Continued

3.3 DEVELOPMENT OF COMPUTATIONAL MODEL

In this project, computational model and simulation of the laser micromachining process is presented using finite element (FE) software. FE software provides a range of modeling and simulation tools to help designers and engineers make decisions earlier in the design process. There are many types of finite element software and for this project, ALGOR simulation software, FEMPRO V22 is used to develop the model and perform simulation. ALGOR simulation software support for multi-CAD environments and extensive finite element modeling tools help manufactures study initial design intent and accurately predict product performance. Moreover, ALGOR had been bench marked for simulating the laser processes.

Computational model consists of defining analysis type, model geometry, mesh design, element type, element definition, material properties and loading. Analysis type that provided in the ALGOR includes linear, nonlinear, thermal, fluid flow, electrostatic, and multiphysics. Thermal analysis type is the option when there is a heat transfer due to conduction, convection, and radiation in individual or combination effect is analyzed. In this project, since the laser micromachining process involving heat transfer process and time factor plays a role, the thermal analysis type with transient heat transfer is chosen. For this analysis type, time steps and load curve are defined due to laser-material interaction. Heat transfer considered in the laser micromachining processing are conduction and convection due to surrounding air.

To develop the governing equations, differential element depicting two-dimensional (2-D) conduction with surface convection as shown in figure 3.2 is referred and the principle of conservation of energy for the differential element is examined.

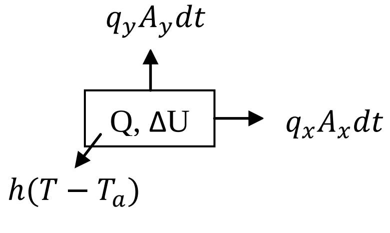

Figure 3.2: Differential element depicting 2-D conduction with convection

The principle of conservation of energy is applied to obtain the governing equation as Eq. (3.1):

$$E_{in} + E_{generated} = E_{increase} + E_{out} \tag{3.1}$$

Eq. (3.1) states that the energy entering the control volume plus energy generated internally by any heat source present must equal the increase in internal energy plus the energy leaving the control volume. For the volume of figure 3.2, during the time intervaldt, Eq. (3.1) is expressed as shown in Eq. (3.2),

$$q_x A_x dt + q_y A_y dt + Q A_x dx dt + Q A_y dy dt = \Delta U + \left(q_x + \frac{\partial T}{\partial x} dx\right) A_x dt + \left(q_y + \frac{\partial T}{\partial y} dy\right) A_y dt + 2h(T - T_a) dx dy \tag{3.2}$$

where q is heat flux, A is area, Q is internal heat generation rate and U is internal energy.

Assuming internal heat generation rate, Q is zero and the change in internal energy ΔU is not zero, the differential equation governing the temperature distribution is shown in Eq. (3.3),

$$k \frac{\partial^2 T}{\partial x^2} + k \frac{\partial^2 T}{\partial y^2} = c\rho \frac{\partial T}{\partial t} + 2h(T - T_a) dx dy \tag{3.3}$$

where k is material thermal conductivity, c is material specific heat, ρ is material density, h is convection coefficient, T is temperature of surface of the body and T_a is ambient fluid temperature.

In developing a finite element approach to two-dimensional conduction with convection, assume a two-dimensional element having M nodes such that the temperature distribution in the element is described by Eq. (3.4),

$$T(x, y, t) = \sum_{i=1}^{M} N_i(x, y) T_i(t) = [N(x, y)]\{T(t)\} \tag{3.4}$$

where $N_i(x, y)$ is the interpolation function associated with nodal temperature T_i, $[N(x, y)]$ is the row matrix of interpolation functions, and $\{T(t)\}$ is the column matrix (vector) of nodal temperatures.

Applying Galerkin's finite element method, the residual equations corresponding to Eq. (3.3) are shown in Eq. (3.5).

$$\iint_A N_i(x,y)\left[k\frac{\partial^2 T}{\partial x^2} + k\frac{\partial^2 T}{\partial y^2} - c\rho\frac{\partial T}{\partial t} - 2h(T - T_a)\right]dA = 0 \quad i = 1, M \tag{3.5}$$

Eq. (3.5) can be generally expressed as Eq. (3.6),

$$\left[C^{(e)}\right]\left\{\dot{T}^{(e)}\right\} + \left[k^{(e)}\right]\left\{T^{(e)}\right\} = \left\{f_g^{(e)}\right\} + \{f_h^{(e)}\} \tag{3.6}$$

where $\left[C^{(e)}\right]$ is the element capacitance and $\left[k^{(e)}\right]$ is the conductance matrix. The forcing function vectors on the right-hand side of Eq. (3.6) include the boundary flux and convection.

Element nodes are assigned to global nodes and the element capacitance matrix terms are added to the appropriate global positions in the global capacitance matrix, as with the conductance matrix terms. Hence, on system assembly, global equation shown in Eq. 3.7 was obtained.

$$[C]\{\dot{T}\} + [K]\{T\} = \{F_g\} + \{F_h\} \tag{3.7}$$

Finite difference method was used to solve finite element formulation. A commonly used approach to obtaining solutions for ordinary differential equations of the form of Eq. (3.7) is the finite difference method. The finite difference method is based on approximating derivatives of a function as incremental changes in the value of the independent variable. The first derivative of a function $f(t)$ is defined by Eq. (3.8).

$$\dot{f} = \frac{df}{dt} = \lim_{\Delta t \to 0} \frac{f(t+\Delta t) - f(t)}{\Delta t} \tag{3.8}$$

Instead of requiring Δt to approach zero, an approximation to the value of the derivative is obtained by using a small, nonzero value of Δt to obtain Eq. (3.9) and the selected value of Δt is known as the time step.

$$\dot{f} \cong \frac{f(t+\Delta t)-f(t)}{\Delta t} \tag{3.9}$$

To apply the procedure to transient heat transfer, the time derivative of the nodal temperature matrix is approximated as shown in Eq. (3.10).

$$\{\dot{T}\} \cong \frac{\{T(t+\Delta t)\}-\{T(t)\}}{\Delta t} \tag{3.10}$$

By substituting Eq. (3.10) into Eq. (3.7), Eq. (3.11) was obtained which shown below.

$$[C]\frac{\{T(t+\Delta t)\}-\{T(t)\}}{\Delta t}+[K]\{T(t)\}=\left\{F_g(t)\right\}+\{F_h(t)\} \tag{3.11}$$

If the nodal temperatures are known at time t and the forcing functions are evaluated at time t, Eq. (3.11) can be solved, algebraically, for the nodal temperatures at time $t+\Delta t$. Denoting the time at the ith time step as $t_i = i(\Delta t)$, i=0,1,2,…, Eq. (3.12) was obtained.

$$[C]\{T(t_{i+1})\}=[C]\{T(t_i)\}-[K]\{T(t_i)\}\Delta t+\left\{F_g(t_i)\right\}\Delta t+\{F_h(t_i)\}\Delta \mathrm{t} \tag{3.12}$$

Model geometry can be either in simple or complex geometry. For ALGOR software, simple geometry such as 2-D geometry can be drawn directly inside the software while complex geometry such as 3-D is needed to draw in solid work and then import to the software for analysis. In this project, the geometry of the computational model is limited to 2-D model. Therefore, the model can be directly constructed inside the software interface. The geometry used for the model is rectangular with the length of 4mm and width of 2 mm.

Proper mesh design would produce accurate and reasonable results, particularly for 2-D and 3-D models. There are two basically types of mesh designs: uniform mesh and selecting finer mesh. Uniform mesh design is used in this project because it gives a more accurate result. The number of division depends on the laser spot size. For validation model, the laser spot size is 0.2 mm. Therefore, the part division is 10 for height and width.

For element type, 4-node plate element is chosen because it is more suitable for 2-D geometry. For material properties, isotropic is selected for material model because the material properties are same in all directions. Integration order is about the accuracy and second (2^{nd}) order is enough for 2-D geometry. In this project, material that used for machining is Polymethyl Methacrylate (PMMA). Since PMMA sheet used in the experiment is 2 mm in thickness, therefore, thickness is defined as 2 mm inside element definition. PMMA properties are obtained from literature or published report and shown in table 3.1.

Table 3.1: Common properties of PMMA

Material properties	PMMA
Density (kg/m^3)	1190
Thermal conductivity ($W\ K^{-1}\ m^{-1}$)	0.17-0.19
Specific heat ($J\ K^{-1}\ kg^{-1}$)	1400-1500
Thermal diffusivity ($x\ 10^{-8}\ m^2\ s^{-1}$)	9.52-11.4
Thermal expansion coefficient ($x\ 10^{-6}\ K^{-1}$)	70-77

Source: Sun (2008)

What types of loads and constraints that will properly define the engineering criteria for the model have to been decided. In finite element analysis (FEA), there are different types of loads and constraints for each analysis type. Applying the proper loads and constraints is one of the most important factors in getting the correct answer. There are multiple ways to apply different loads and constraints to a model such as nodal, edge, surface and element.

As involved in laser micromachining are conduction and convection heat transfer, the former was computed through nodal heat flux and the latter through surface convection load. Nodal heat source represent the power from the laser source that used for machining PMMA. The computational is done at the center line of the model. For validation model, the laser power, spatial velocity and spot size are 1 W, 50 mm/min and 0.2 mm respectively. Laser spot size and spatial velocity are controlled by activation time and smallest nodal distance along the processing line.

Some assumptions were made in finite element modeling. Ambient temperature during laser processing was assigned to be at 25 °C. It is hard to know the exact convection coefficient during the laser micromachining process. Therefore, the value of convection coefficient is estimated as 0.02 $J/(s \cdot deg\ C \cdot mm^2)$. Besides, properties for PMMA are assumed because there is a range of values that found in the internet source.

3.4 SIMULATION OF LASER MICROMACHINING

Designed experiments approach is superior over other approaches because it is a systematic and scientific way of planning the experiments, collection and analysis of data with limited use of available resources. In this project, laser micromachining was simulated for varying laser parameters. Parameter setting was designed using design of experiment (DOE) available in STATISTICA. 3**K was full factorial design where 3 is level and K is number of factors.

The process parameters and range in simulations are as follows:

i. Laser power, P; $0.02 \leq P\ (W) \leq 0.50$
ii. Spatial velocity, V; $10 \leq V\ (mm/min) \leq 50$
iii. Spot size, d; $0.10 \leq d\ (mm) \leq 0.4$

The complete parameter setting which generated by the STATISTICA software is shown in the figure 3.3. It was assumed that computer processing performance would be repeatable and order of simulation would not affect the results. Consequently, randomization and replication was not included in the design of experiment (DOE).

Standard Run	P	V	d
	3**(3-0) full factorial design, 1 block , 27 runs (Spreadsheet3)		
8	0.020000	50.00000	0.250000
4	0.020000	30.00000	0.100000
2	0.020000	10.00000	0.250000
14	0.260000	30.00000	0.250000
6	0.020000	30.00000	0.400000
7	0.020000	50.00000	0.100000
3	0.020000	10.00000	0.400000
5	0.020000	30.00000	0.250000
17	0.260000	50.00000	0.250000
22	0.500000	30.00000	0.100000
10	0.260000	10.00000	0.100000
24	0.500000	30.00000	0.400000
27	0.500000	50.00000	0.400000
1	0.020000	10.00000	0.100000
16	0.260000	50.00000	0.100000
20	0.500000	10.00000	0.250000
25	0.500000	50.00000	0.100000
21	0.500000	10.00000	0.400000
26	0.500000	50.00000	0.250000
13	0.260000	30.00000	0.100000
18	0.260000	50.00000	0.400000
11	0.260000	10.00000	0.250000
12	0.260000	10.00000	0.400000
19	0.500000	10.00000	0.100000
9	0.020000	50.00000	0.400000
15	0.260000	30.00000	0.400000
23	0.500000	30.00000	0.250000

Figure 3.3: Design of Experiment generated by STATISTICA

3.5 RESULT ANALYSIS

There are various analysis options in STATISTICA software. In this project, model, residual plots, ANOVA/Effects, prediction and profiling are going to be discussed. For model, no interactions or 2-way interactions (linear, quadratic) that include in model were considered. For each interaction that include in model, the ANOVA table, the normal plot and observed vs. predicted values which under residual plots are observed. Between these two interactions, the one that gives the better result will be chosen as the interactions that include in model. After that, the surface/contours plot is generated to identify the feasible process parameter for laser micromachining.

CHAPTER 4

RESULT AND DISCUSSION

4.1 INTRODUCTION

This chapter will discuss about the result and discussion of this project. For this project, the result is obtained from ALGOR software to measure the size of measured cutting zone, s. To ensure that the computational model and simulation of this process is acceptable, the result is compared with the experimental result that done by others.

After validation, simulation is done for the design of experiment (DOE) that generated by STATISTICA software. Since there are three independent variables, there are total 27 simulations that have to be done. The results are then analyzed by using STATISTICA software. Throughout this chapter, the effect of power, velocity and spot size on the size of measured cutting zone will be discussed.

4.2 COMPUTATIONAL MODEL

Analysis type that used for this model was thermal analysis with transient heat transfer. Transient heat transfer analysis was chosen to predict time-resolved temperature distribution in the material due to laser pulse. Material model considered was isotropic because the material properties are constant in all direction. The element type was plate element. Material properties are custom defined as PMMA is not includes in built-in material library available in ALGOR.

Figure 4.1 shows the model geometry which had been constructed for simulation.

Figure 4.1: Model Geometry (4 mm x 2 mm)

The most important part of the FE modeling was mesh design including the nodal distance along the laser path and node order as the laser would follow these. As a straight cut would be simulated, it was essential that the nodes in the computational domain would follow a straight path. The nodal distance along the laser path was modeled to be the length of 0.2 mm each. Laser beam was represented by nodal heat source and activation time which was defined consistently with load curve. Laser power was defined based on the frequency and moving velocity. Laser spatial velocity was controlled by nodal distance and activation time.

Figure 4.2 shows the model with uniform mesh design.

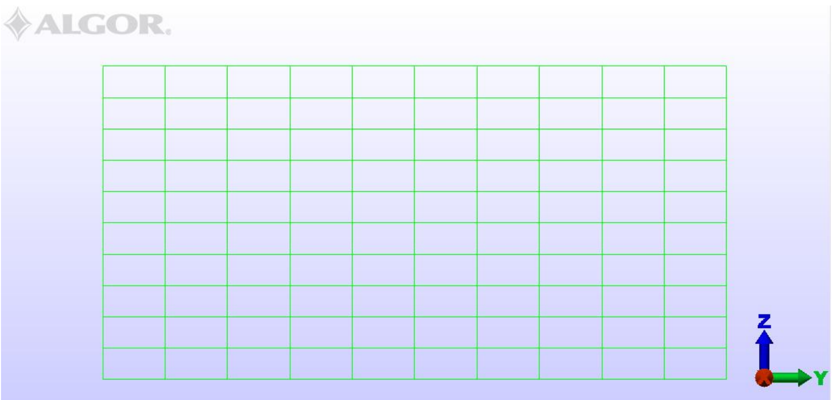

Figure 4.2: Model with uniform mesh design

Surface convection heat coefficient was assigned to include convection heat transfer due to surrounding air. Initial nodal temperature was assigned to be at 25 °C assuming the laser processing at room temperature. The value for the convection coefficient is one of the assumptions that had been made too. This is because it is hard to know the exact convection coefficient during the laser micromachining process. In this project, the convection coefficient is estimated as 0.02 J/(s·deg C·mm^2). Figure 4.3 shows the model with surface convection load.

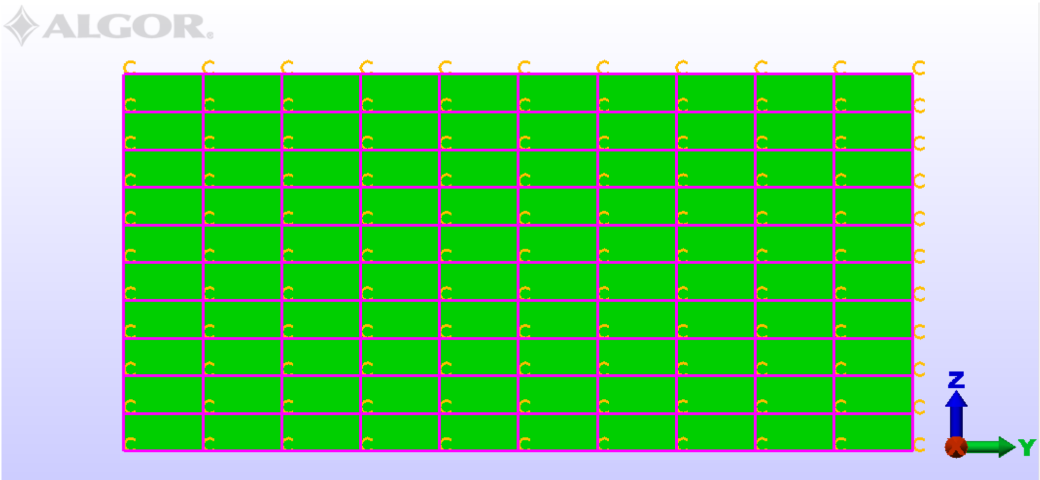

Figure 4.3: Model with surface convection load

The laser interaction time with PMMA is defined by a load curve as shown in figure 4.4.

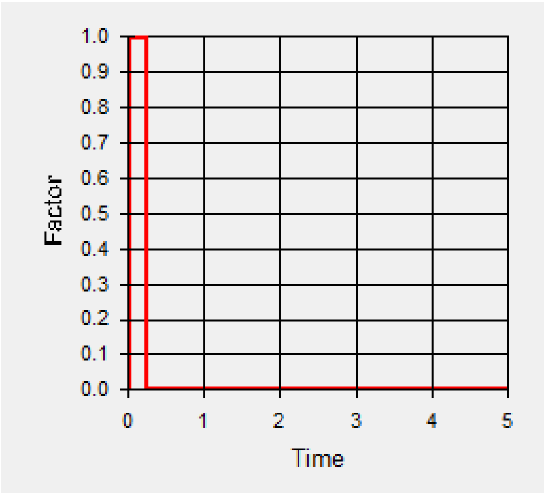

Figure 4.4: Load curve for defining laser interaction

Figure 4.5 shows complete model for computation. It highlights element geometry, number of elements, load and boundary condition, and direction of nodal heat flux. The arrow shows the direction of laser path during laser micromachining process.

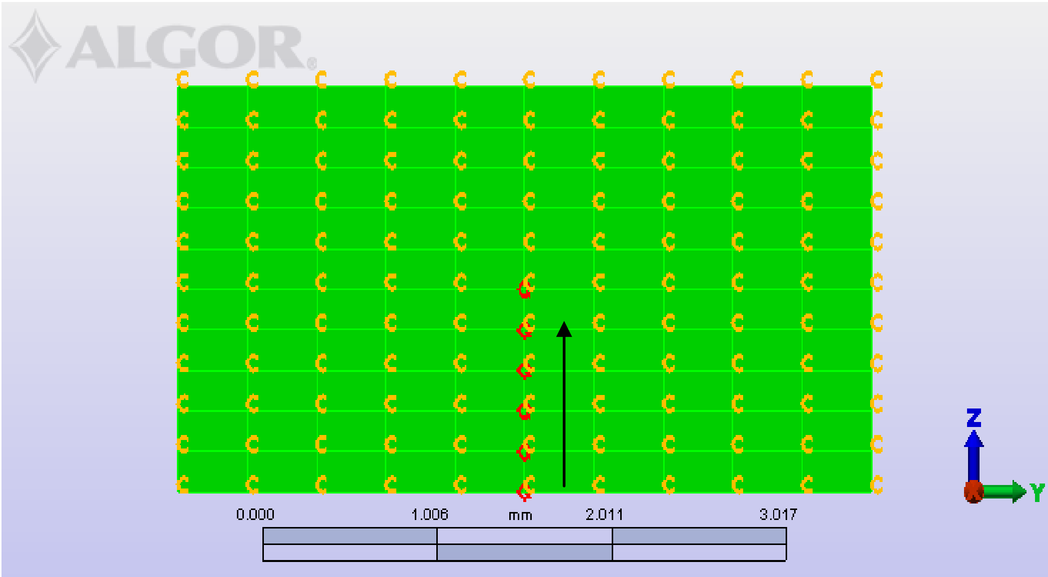

Figure 4.5: Complete model for computation

After compute the model, analysis is performed and the result is evaluated. The contour plot by colour band and the temperature distribution during laser micromachining are observed. In order to obtain the size of major cutting zone, result in contour plot by isolines is used to get the measurement.

4.3 MODEL VALIDATION

For validation purpose, simulation result is compared with the experimental result that done by others. With the same processing parameter, the size of major cutting zone that obtained by simulation and experimental is compared. If the size difference between the simulation and the experimental is less than 10 %, then the simulation result is validated. This means that the use of finite element (FE) modeling and simulation is the right tool to meet the requirement.

Initial simulation result was carried out to validate the model. Figure 4.6 shows the simulation result for the model.

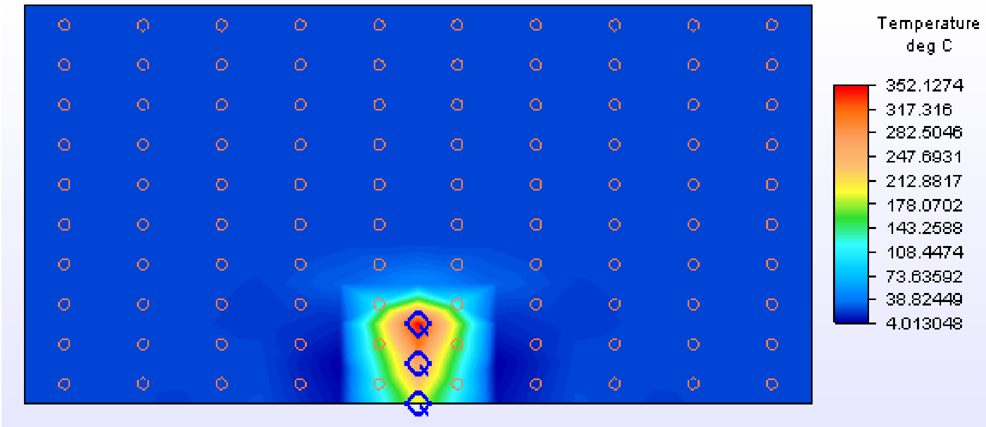

Figure 4.6: Temperature contour simulated in colour band

From this simulation result, contour plot and temperature distribution during laser micromachining can be observed. Temperature colour band shows that red colour is the region where the highest temperature had been occurred. This region is where the material is removed by the laser source. In order to measure the size for major cutting zone where the temperature exceeds the melting point of PMMA, contour plot by isolines is generated as shown in the figure 4.7.

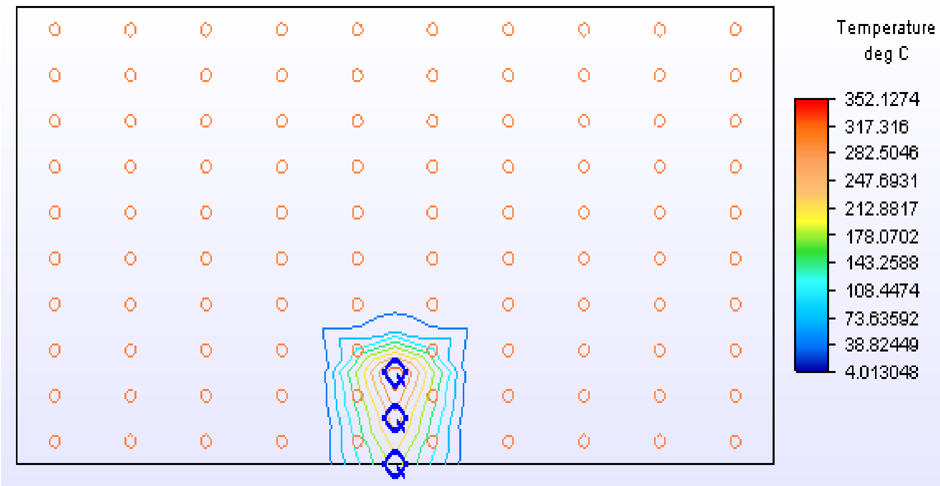

Figure 4.7: Temperature contour simulated in isolines

Through this contour plot, the size of major cutting zone is where the temperature exceeds the melting temperature of the PMMA and therefore the material is removed by the laser source. The size is measured by the width of that region which can be shown clearly in the contour plot by isoline in ALGOR software. From this result, the size of major cutting zone, s, is 162 µm. This means that 162 µm of PMMA is removed during laser micromachining process.

In order to verify the above result, the experimental result with same parameter set as simulation was investigated. Figure 4.8 depicts micrograph of cutting zone on PMMA generated by Nd-YAG laser. The arrow shows the direction of laser path.

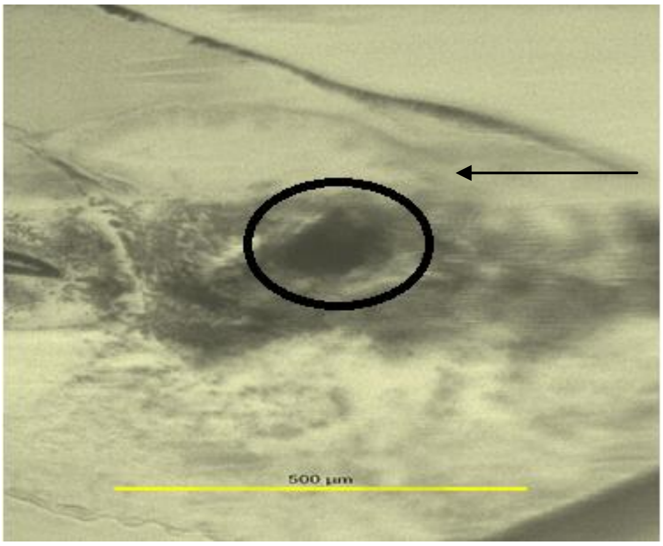

Figure 4.8: Micrograph of cutting zone on PMMA

The darkest region that had been circled in the figure shows the maximum temperature that occurred during the process. This region is where the material is removed by the laser source. The size of major cutting zone, s, is 154 µm.

The error percentage when comparing the simulation result with experimental result is 5.19 %. Computational model is validated since the error percentage is less than 10 %.

4.4 SIMULATION FOR VARIOUS PARAMETERS

The laser power, P, spatial velocity, V, and spot size, d, are the three independent variables and the size of the measured cutting zone, s, is the dependent variable in this project. After simulate each different combination of the independent variables, the result which is the size of the major cutting zone is obtained. There were total 27 numbers of simulations done based on design of experiment (DOE) generated by the STATISTICA software.

From the simulation result, heat propagation through the PMMA and the contour of heat affected zone (HAZ) can be observed. Three out of 27 simulations were chosen to investigate detail physical performance which distinctly shows the heat propagation through the material. The remaining contour results are shown in the Appendix.

4.4.1 Power = 0.5 W, spatial velocity = 30 mm/min and spot size = 0.10 mm

First simulation result with the parameter of power = 0.5 W, spatial velocity = 30 mm/min and spot size = 0.10 mm is shown. The temperature contour colour band simulated is shown in the figure 4.9 and temperature contour by isolines is shown in the figure 4.10.

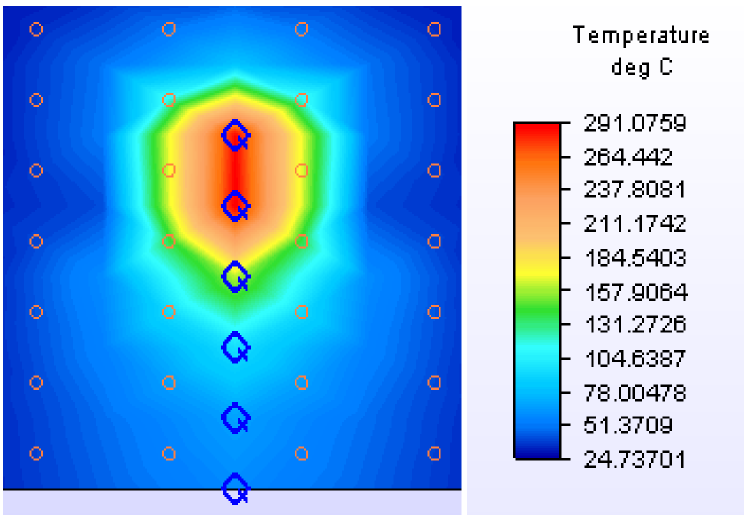

Figure 4.9: Temperature contours simulated in colour band

This contour plot shows how the heat is propagated through the material. The red colour band is where the highest temperature occurs. The melting temperature for PMMA is in the range of 130-157 °C. Therefore, the region with temperature within or above this range will remove by the laser source. This region is called the size of measured cutting zone. The size can be measured using the contour plot by isolines as shown in the figure. From the contour plot, the two nodes are continuous during the laser micromachining. This is desirable during the process as the size of major cutting zone is even and the heat affected zone can be minimized. In term of cutting zone, this result shows a positive result. It likely produces a good cut quality.

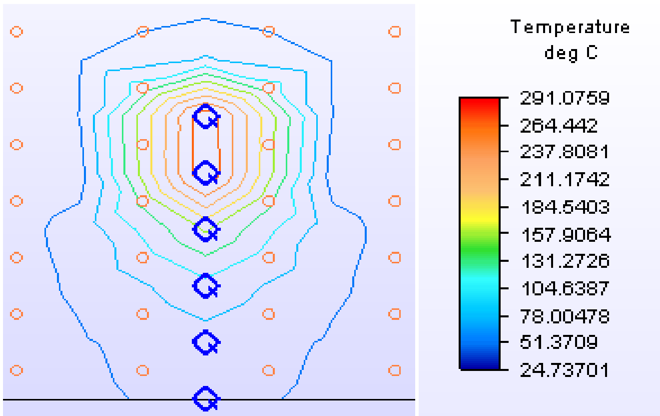

Figure 4.10: Temperature contour simulated in isolines

Contour plot by isolines can show clearly how the heat propagates into the material. The heat propagation is considered consistent during the laser micromachining process. The size of the cutting zone was measured perpendicularly with the direction of the laser beam. The region which has the temperature within or higher than the melting temperature of PMMA is included in the size of measured cutting zone. This simulation has the size of major cutting zone of 215 µm.

4.4.2 Power = 0.26 W, moving velocity = 10 mm/min and spot size = 0.25 mm

Second simulation result with power = 0.26 W, moving velocity = 10 mm/min and spot size = 0.25 mm is shown in the figure 4.11 and figure 4.12. Figure 4.11 shows temperature contour simulated in colour band while figure 4.12 shows the temperature contour simulated in isolines.

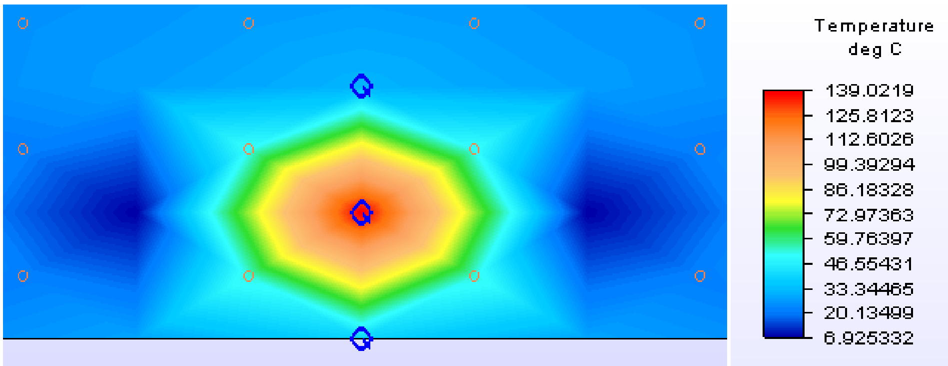

Figure 4.11: Temperature contour simulated in colour band

The contour plot shows that the heat propagation through PMMA is very wide and thus, the heat affected zone (HAZ) is large. This is not desired because the surface roughness is not good and will affect the appearance of the material. There is no continuous laser cutting compared with the first simulation result shown in figure 4.9.

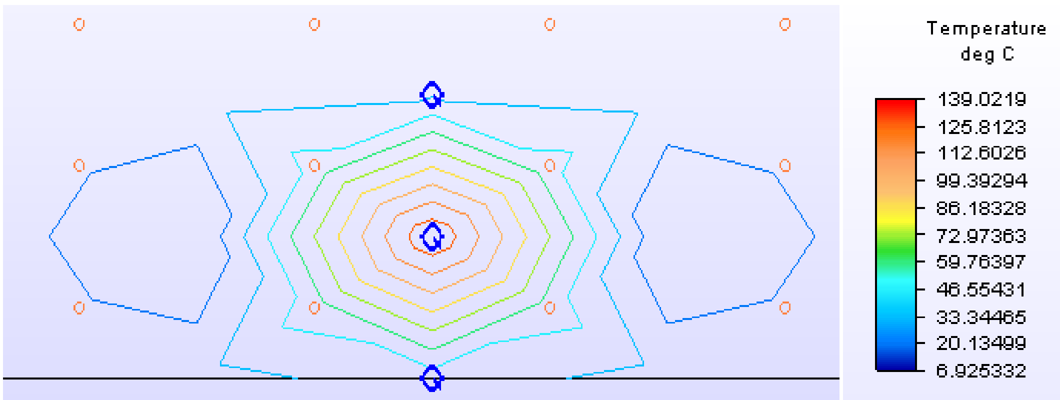

Figure 4.12: Temperature contour simulated in isolines

From the temperature contour simulated in isolines, the size of the major cutting line is 100 µm. Although the heat propagation is large, it has the smaller size of major cutting zone compared with first simulation. This is because the laser power used in this simulation is smaller.

4.4.3 Power = 0.5 W, moving velocity = 50 mm/min and spot size = 0.25 mm

Third simulation result with power = 0.5 W, moving velocity = 50 mm/min and spot size = 0.25 mm is shown in the figure 4.13 and figure 4.14. Figure 4.13 shows temperature contour simulated in colour band while figure 4.14 shows the temperature contour simulated in isolines.

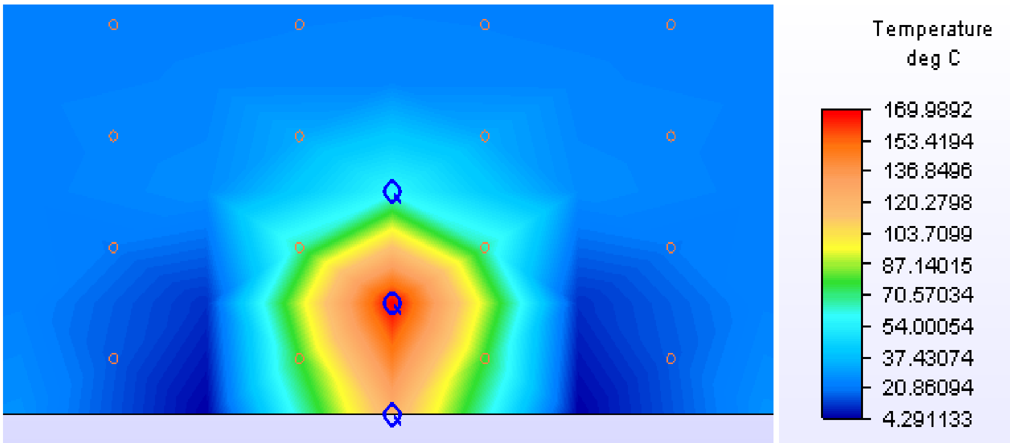

Figure 4.13: Temperature contour simulated in colour band

The heat propagation through PMMA for this simulation is quite wide. Therefore, the HAZ is large but smaller compared to the second simulation result. The laser cutting using these combination parameters is still considered continuous. The red region which has the highest temperature is very small.

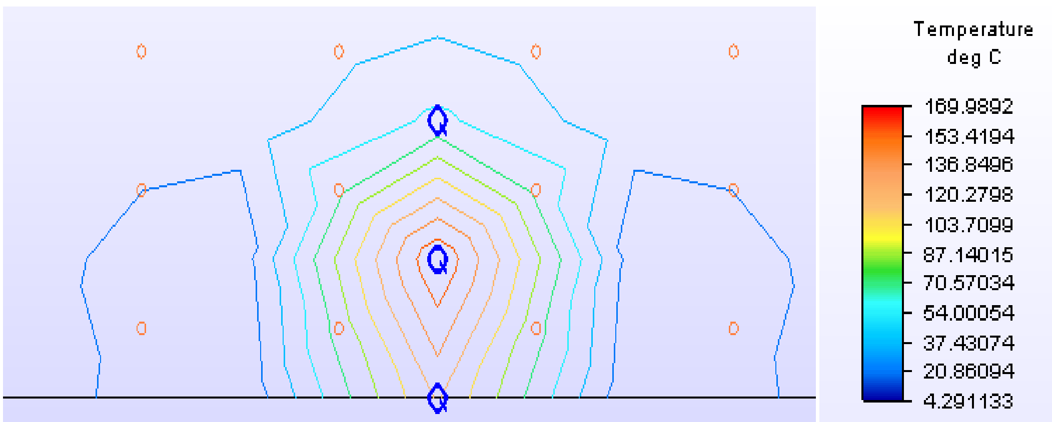

Figure 4.14: Temperature contour simulated in isolines

With isolines contour plot, the heat propagation throughout the process can be seen clearly. If compared with the second simulation result, the heat propagation in this simulation result is not as wide as the second simulation. However, the size of measured cutting zone is bigger which is 209 µm. This is because the power used for this simulation is higher which is 0.5 W.

4.5 ANALYSIS USING STATISTICA SOFTWARE

The simulation result is analyzed by the analysis option that provided in STATISTICA software. Figure 4.15 shows the design of experiment table with the result.

Data: Spreadsheet8* (4v by 27c)

	1 P(W)	2 V(mm/min)	3 d(mm)	4 s(µm)
1	0.020	50.000	0.250	0.001
2	0.020	30.000	0.100	0.001
3	0.020	10.000	0.250	0.001
4	0.260	30.000	0.250	94.000
5	0.020	30.000	0.400	0.001
6	0.020	50.000	0.100	0.001
7	0.020	10.000	0.400	0.001
8	0.020	30.000	0.250	0.001
9	0.260	50.000	0.250	0.010
10	0.500	30.000	0.100	215.000
11	0.260	10.000	0.100	121.000
12	0.500	30.000	0.400	142.000
13	0.500	50.000	0.400	155.000
14	0.020	10.000	0.100	0.001
15	0.260	50.000	0.100	400.000
16	0.500	10.000	0.250	280.000
17	0.500	50.000	0.100	300.000
18	0.500	10.000	0.400	323.000
19	0.500	50.000	0.250	209.000
20	0.260	30.000	0.100	87.000
21	0.260	50.000	0.400	0.010
22	0.260	10.000	0.250	100.000
23	0.260	10.000	0.400	0.010
24	0.500	10.000	0.100	280.000
25	0.020	50.000	0.400	0.001
26	0.260	30.000	0.400	0.010
27	0.500	30.000	0.250	296.000

Figure 4.15: Design of experiment table with the result

4.5.1 Analysis model

First of all, a suitable model needs to be chosen. For the analysis principals, there are two model option, which is no interactions model or 2-way interactions (linear, quadratic) model. In order to identify significant effect and feasible parameter combination, no interactions model is desirable because it make the analysis simple. However, both model options were analyzed and the model that give a better analyzed result will be chosen for determination of significant factor and parameter combination.

Figure 4.16 shows the ANOVA that generated for no interactions model.

ANOVA; Var.:s(µm); R-sqr=.7142; Adj:.62846 (Spreadsheet8)
3 3-level factors, 1 Blocks, 27 Runs; MS Residual=6288.958
DV: s(µm)

Factor	SS	df	MS	F	p
(1)P(W) L+Q	275463.2	2	137731.6	21.90054	0.000009
(2)V(mm/min) L+Q	4718.7	2	2359.3	0.37515	0.691918
(3)d(mm) L+Q	34136.2	2	17068.1	2.71398	0.090612
Error	125779.2	20	6289.0		
Total SS	440097.2	26			

Figure 4.16: ANOVA table for no interactions model

From the ANOVA table, the R-square value is 0.7142 which is less than 0.8. This means that model with no interactions is not a good fit of the data. The laser power has the most significant effect to the dependent variable which is the size of measured cutting zone because it has p value less than 0.05. According to ANOVA table, the laser velocity and laser spot size have no significant effect to the size of measured cutting zone. However, laser spot size with p value close to 0.05 has more effect compared with laser moving velocity. Therefore, the most significant effect is laser power, followed by laser spot size and laser moving velocity. However, it is just a theory and is not always true for every process.

After interpret the ANOVA table, normal probability plots of residuals is observed and discussed. Figure 4.17 shows the normal plot for no interactions model.

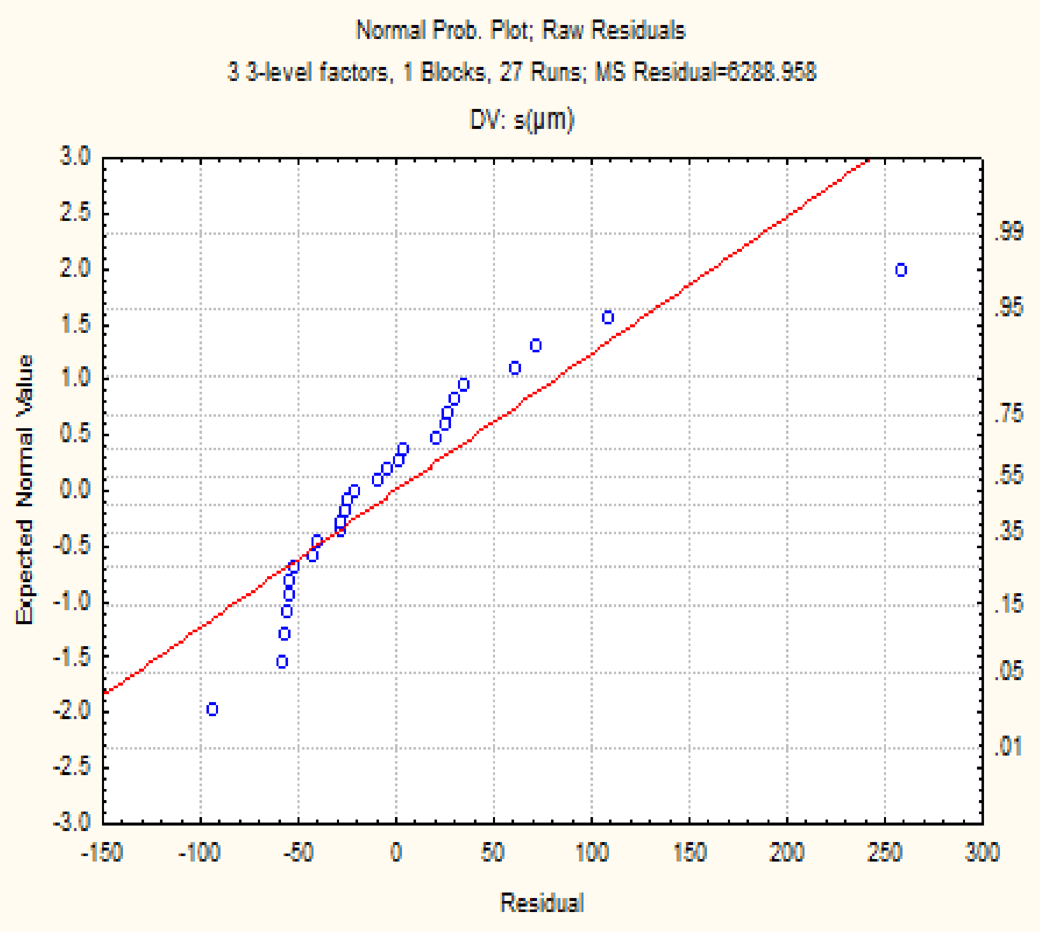

Figure 4.17: Normal probability plots of residual for no interactions model

The blue point is the result values that obtained in simulation while the red line is the normal values. Through this normal plot, conclusion can be made where the result given by model with no interactions is not fit on the normal line but quite far from the normal line. So, the accuracy of the result is reduced.

In addition to the normal probability residuals plot, scatter plots for observed versus predicted values is also evaluated. The observed versus predicted values scatter plots is shown in the figure 4.18.

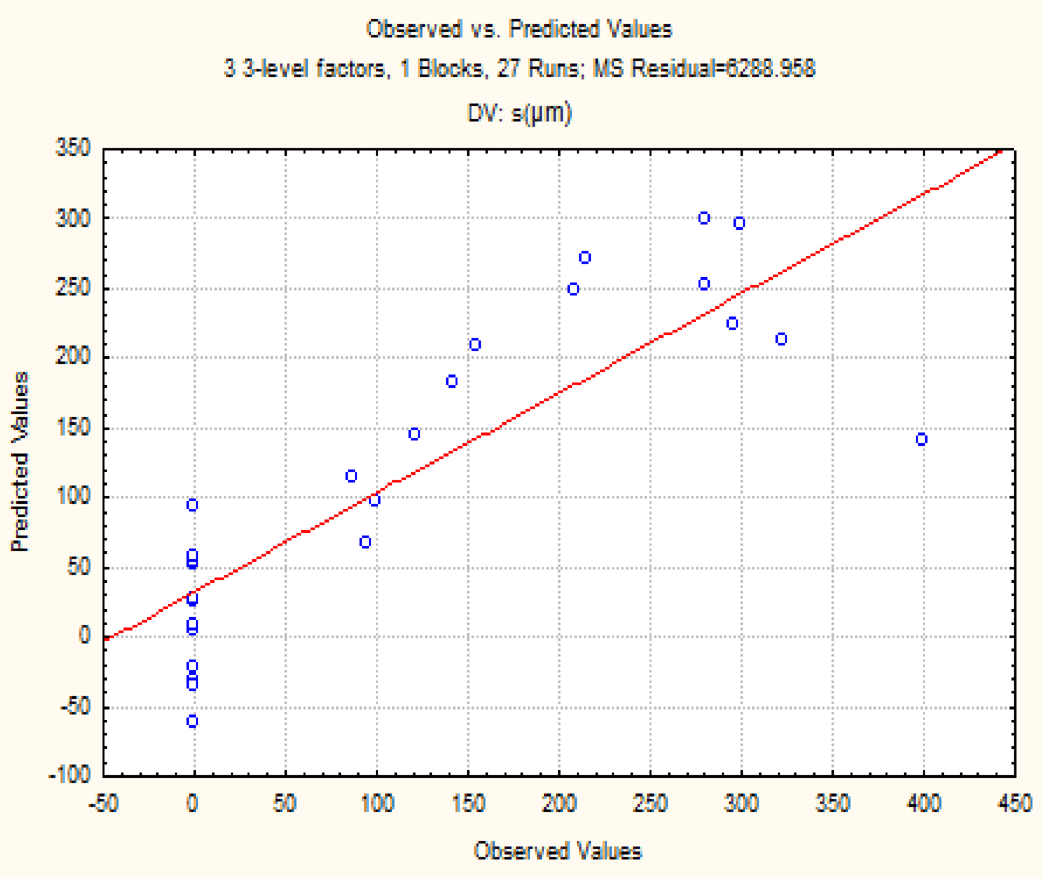

Figure 4.18: Observed versus predicted values scatter plots for no interactions model

Observed versus predicted values scatter plots is used to determine whether the predicted value that generate according to the results obtained has the relationship with the actual results or not. The blue point is the results values obtained while the red line is the predicted value generated by STATISTICA software. The plots show that most of the results value obtained are far from the predicted values. This can mean that the results value that obtained is not that accurate.

After done the analysis for no interactions model, model with 2-ways interactions (linear, quadratic) is going to be analyzed. The ANOVA that generated by 2-way interactions (linear, quadratic) model is shown in the figure 4.19.

ANOVA table shows that the R-square value is 0.91817 which is more than 0.8. This means that this model is a good fit of the data. Therefore, 2-way interactions (linear, quadratic) model is better than no interactions model.

ANOVA; Var.:s(μm); R-sqr=.91817; Adj:.73404 (Spreadsheet8)
3 3-level factors, 1 Blocks, 27 Runs; MS Residual=4501.852
DV: s(μm)

Factor	SS	df	MS	F	p
(1)P(W) L+Q	77444.2	2	38722.12	8.601374	0.010152
(2)V(mm/min) L+Q	18745.3	2	9372.65	2.081954	0.187097
(3)d(mm) L+Q	34136.2	2	17068.08	3.791345	0.069469
1*2	15569.3	4	3892.33	0.864607	0.524470
1*3	36596.5	4	9149.11	2.032300	0.182534
2*3	37598.6	4	9399.64	2.087949	0.174343
Error	36014.8	8	4501.85		
Total SS	440097.2	26			

Figure 4.19: ANOVA table for 2-way interactions (linear, quadratic) model

Laser power has the p value which less than 0.05 while laser moving velocity and laser spot size has the p value which more than 0.05. Parameter with p value less than 0.5 means it has the significant effect on the dependent variable. Inversely, parameter with p value more than 0.5 means it has no significant effect on the dependent variable. According to ANOVA table, the laser power has the most significant effect on the size of measured cutting zone and laser velocity and laser spot size have less effect on the size of measured cutting zone. The p value for laser spot size is near to 0.05. Therefore, laser spot size has more effect compared with laser moving velocity.

After interpret the ANOVA table, normal probability plots of residuals is observed and discussed. Figure 4.20 shows the normal plot for no interactions model.

From this normal plot, most of the result values that obtained are fit on the normal line. There are only certain points which are far from the normal line. Thus, 2-way interactions (linear, quadratic) model give a better normal plot compare with no interactions model.

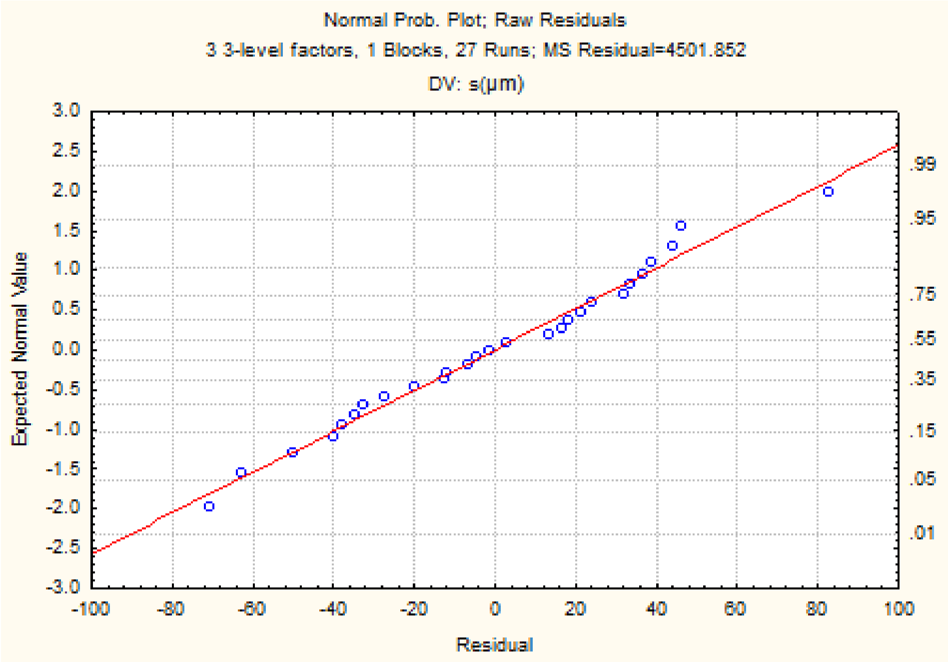

Figure 4.20: Normal probability plots of residual for 2-way interactions model

Scatter plots for observed versus predicted values is evaluated. The observed versus predicted values scatter plots is shown in the figure 4.21.

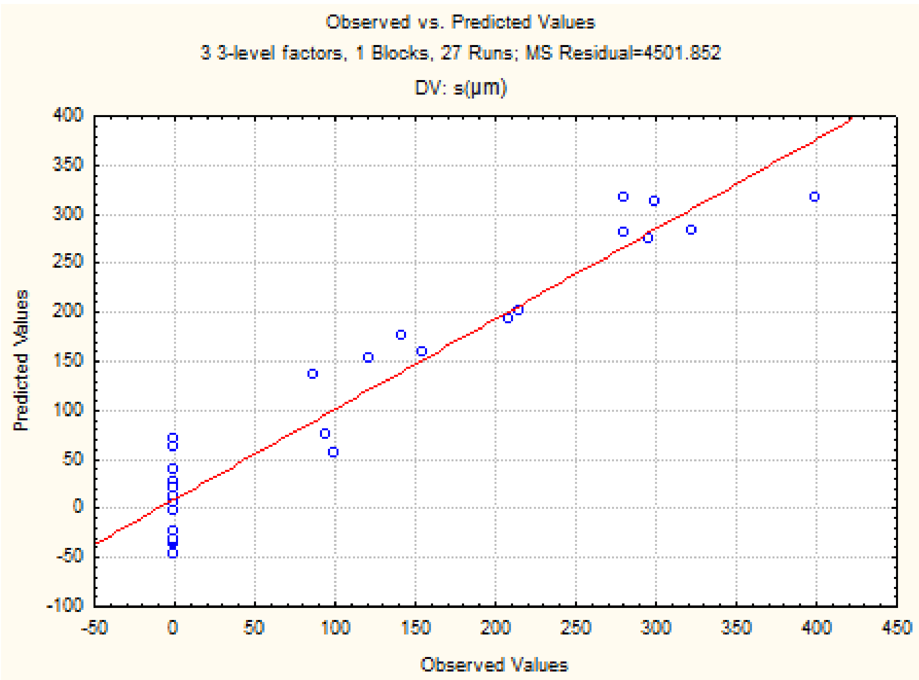

Figure 4.21: Observed versus predicted values scatter plots for 2-way interactions

Observed versus predicted values scatter plots allows the comparison value between the result obtained with the actual result that generated by the STATISTICA software. The blue point is the results values obtained while the red line is the predicted value generated by STATISTICA software according to the results values obtained. The plots shows some results value obtained are far from the predicted values. However, when compared with no interactions model, 2-way interactions (linear, quadratic) model gives the better analysis.

Since 2-way interactions (linear, quadratic) model provide a better R-square value, better normal probability plots of residuals and better observed versus predicted values scatter plots, it is chosen as the model to analyze.

4.5.2: Desirability surface/contours

After the better model interactions was chosen, the desirability surface/contours was observed to determine the parameter combination used for laser micromachining for machining PMMA. Figure 4.22 shows the desirability surface/contours that generated by the STATISTICA software.

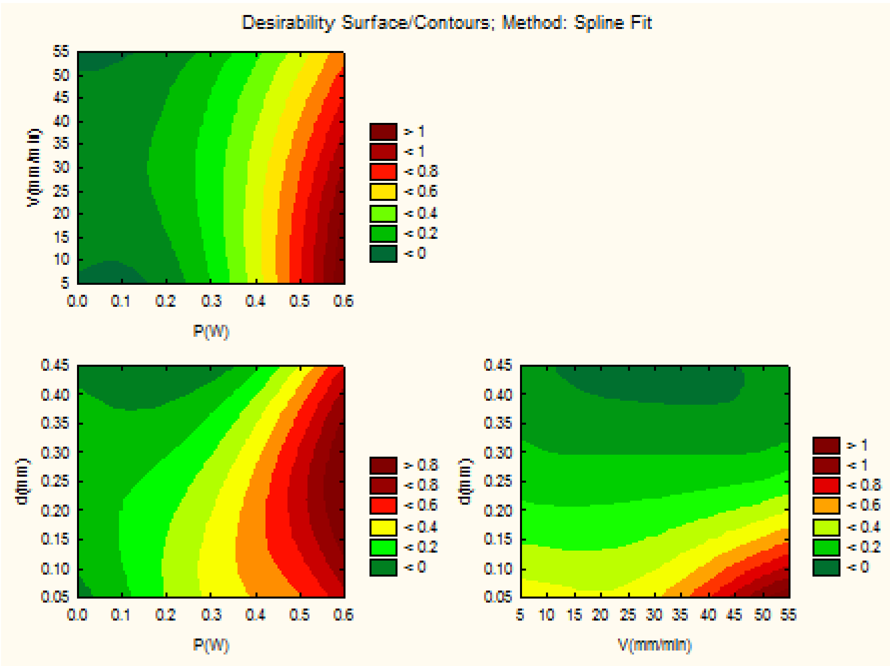

Figure 4.22: Desirability surface/contours

The region where the combination parameter can produce the minimum size of measured cutting zone is desirable. Surface/contours region that with <0 value means a negative value and it is meaningless. Therefore, surface/contours with <0.2 was observed and the better parameter combination is determined.

During the laser micromachining process, the size of measured cutting zone is not desirable. Therefore, combination parameters used during the laser micromachining process must be appropriated to make sure the size of measured cutting zone is as small as possible. In this project, the combination parameters include laser power, laser moving velocity and laser spot size. According to the surface/contours plot in figure 4.22, combination parameters where the power is within the range of 0-0.3 W, the spot size is > 0.15 mm, and the velocity is in the range of 5-55 mm/min will produce small size of measured cutting zone. This can be a useful guideline for choosing the appropriate parameters during laser micromachining process for machining PMMA in order to minimize the size of major cutting zone.

CHAPTER 5

CONCLUSION AND RECOMMENDATIONS

5.1 CONCLUSION

Computational model has been successfully developed for simulating laser micromachining of Polymethyl Methacrylate (PMMA) material. The model had been validated with the experimental result. From the simulated results, proper compromise between three independent variable: laser power, laser moving velocity and laser spot size would be essential in order to minimize the size of measured cutting zone during laser micromachining process.

The important factors for realistic simulation of laser micromachining include mesh design in FE modeling, appropriate material model, accurate thermal properties of material under processing and boundary condition used. All these affected the simulation results considerably.

Referring to statistical analysis, laser power was found to be the most significant effect to the size of measured cutting zone, followed by laser spot size and spatial velocity. Predicted parameters that should be used during laser micromachining for machining PMMA are: laser power within the range of 0-0.3 W, laser spot size > 0.15 mm and laser moving velocity in the range of 5-55 mm/min.

5.2 RECOMMENDATIONS

Laser micromachining has many technological advantages compared to conventional technologies. Therefore, laser micromachining process had been widely used nowadays. Since the experimental work of laser micromachining is costly and time consuming, computational model and simulation of this process are preferred. It can be helpful to predict appropriate process parameters that enable to produce high quality products. Adequate prior simulations are mandatory to save time and cost of real production. In this project, the finite element (FE) software used is ALGOR. Thus, a study on other FE software should be done. This is because there might be other FE software that can provide more accurate results for simulating the laser micromachining process.

There are numerous parameters involved in laser micromachining processing. However, in this project, there are only three parameters are discussed which include the laser power, laser spot size and laser velocity. Therefore, a research on others parameters should be done so that the quality of the products can be increased.

Nowadays, Polymethyl Methacrylate (PMMA) is widely used as it is a versatile thermoplastic that is well suited for engineering and many common applications. More research on feasible laser micromachining parameter for PMMA is required to produce the good surface finish of PMMA.

REFERENCES

Abgrall, P. and Nguyen, N. 2009. *Nano fluidics.* USA: Artech House.

Agrawal, G.P. and Dutta, N.K. 1986. *Long wavelength semiconductor lasers*. New York: Van Nostrand Reinhold.

Aldrich, R. (undated). Laser Fundamentals (online). http://www.fas.org/man/dod-101/navy/docs/laser/fundamentals.htm#LASER TYPES (11 August 2009)

Arieli, R. (undated). Laser Adventure (online). http://stwww.weizmann.ac.il/Lasers/laserweb/Ch-6/F6s3p1.htm (15 August 2009)

Azojomo Azo Journal of Materials Online. 2010. Software (online) http://www.azom.com/engineering_software.asp?cat=11 (5 October 2010)

Caiazzo, F., Curcio, F., Daurelio G. and Memola, F.C.M. 2005. Laser cutting of different polymeric plastics (PE, PP and PC) by a CO_2 laser beam. *Journal of Material Processing Technology*. **159**(3): 279–285.

Chen, M.F., Wang, Y.H. and Hsiao, W.T. 2009. Finite element analysis and verification of laser marking on eggshell. *Journal of Material Processing Technology*. **209**(1): 470-476.

Cheng, J.Y., Wei, C.W., Hsu, K.H. and Young, T.H. 2004. Direct-write laser micromachining and universal surface modification of PMMA for device development. *Sensors and Actuators B: Chemical*. **99**(1): 186-196.

Davim, J.P., Barricas, N., Conceiçao, M. and Oliveria, C. 2008. Some experimental studies on CO_2 laser cutting quality of polymeric materials. *Journal of Material Processing Technology.* **198**(1-3): 99–104.

Davim, J.P, Oliveria, C., Barricas, N. and Conceiçao, M. 2008. Evaluation of cutting quality of PMMA using CO_2 lasers. *International Journal of Advanced Manufacturing Technology*. **35**(9-10): 875-879.

Dubey, A.K. and Yadava, V. 2008. Experimental study of Nd:YAG laser beam machining-An overview. *Journal of Materials Processing Technology*. **195**(1-3): 15-26.

Eidgenossische Technische Hochschule Zurich. 2006. Materials for you (online). http://www.materials4u.ethz.ch/inform/materials/pmma/index_EN (5 August 2009).

Elijah, K.A. 2009. *Principles of laser materials processing.* Canada: John Wiley & Sons, Inc.

Geschke, O., Klank, H. and Telleman, P. 2004. *Microsystem engineering of lab-on-a-chip* devices. Germany: Federal Republic.

Huang, y., Liu, S., Yang, W. and Yu, C. 2010. Surface roughness analysis and improvement of PMMA-based microfluidic chip chambers by CO_2 laser cutting. *Appiled Surface Science*. **256**(6): 1675-1678.

Hutton, D.V. 2004. *Fundamentals of finite element analysis*. USA: McGraw-Hill.

Jensen, M.F., Noerholm, M., Christensen, L.H. and Geschke, O. 2003. Microstructure fabrication with a CO2 laser system: Characterization and fabrication of cavities produced by raster scanning of the laser beam. *Lab on a chip – Miniaturisation for Chemistry and Biology*. **3**(4): 302-307.

Kim, M.J. and Zhang, J. 2001. Finite element analysis of evaporative cutting with a moving high energy pulsed laser. *Applied Mathematical Modeling*. **25**(3): 203-220.

Klank, H., Kutter, J.P. and Geschke, O. 2002. CO_2-laser micromachining and back-end processing for rapid production of PMMA-based microfluidic systems. *Lab On a Chip*. **2**(4): 242-246.

Liu, K. 1996. *Development of a laser-based surface finishing tool*. Ph.D. Thesis. University of California at Berkeley, US.

McGeough, J. 2002. *Micromachining of engineering materials*. New York: Marcel Dekker, Inc.

Meijer, J., 2004. Laser beam machining (LBM), state of the art and new opportunities. *Journal of Material Processing Technology*. **149**(1-3): 2–17.

Michael, G. 2006. *Finite element method: applications in solids, structures, and heat transfer*. Boca Raton: Taylor & Francis Group.

Norikazu, T., Shigenori, Y. and Masao, H., 1996. Present and future of lasers for fine cutting of metal plate. *Journal of Material Processing Technology*. **62**(4): 309–314.

Pryputniewicz, R.J., Han, W. and Nowakowski, K.A. 2006. New approach of synthesis of laser microwelding processes for packaging. *1T4. Fatigue and Fracture of MEMS and NEMS*. 73-74.

Yang, J., Sun, S., Brandt, M. and Y, W. 2010. Experimental invertigation and 3D finite elemnt prediction of the heat affected zone during laser assisted machining of Ti6Al4V alloy. *Journal of Materials Processing Technology*. **210**(15): 2215-2222.

Zhou, B.H. and Mahdavian, S.M. 2004. Experimental and theoretical analyses of cutting nonmetallic materials by low power CO_2 - laser. *Journal of Material Processing Technology*. **146**(2): 188–192.

APPENDIX A

SIMULATION RESULTS FOR VARIOUS PARAMETER COMBINATIONS

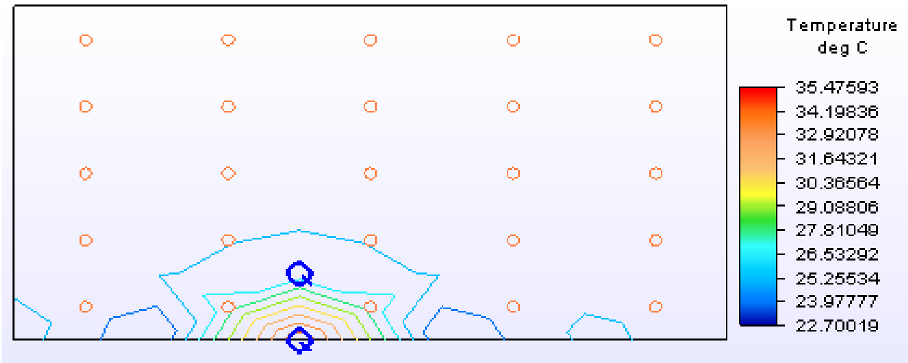

Figure 6.1: Temperature contour simulated in isolines for parameter combinations of power = 0.02 W, spatial velocity = 10 mm/min and spot size = 0.40 mm

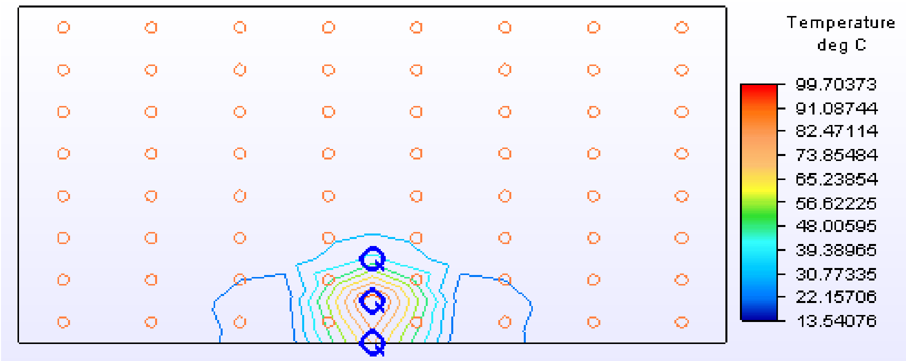

Figure 6.2: Temperature contour simulated in isolines for parameter combinations of power = 0.26 W, spatial velocity = 50 mm/min and spot size = 0.25 mm

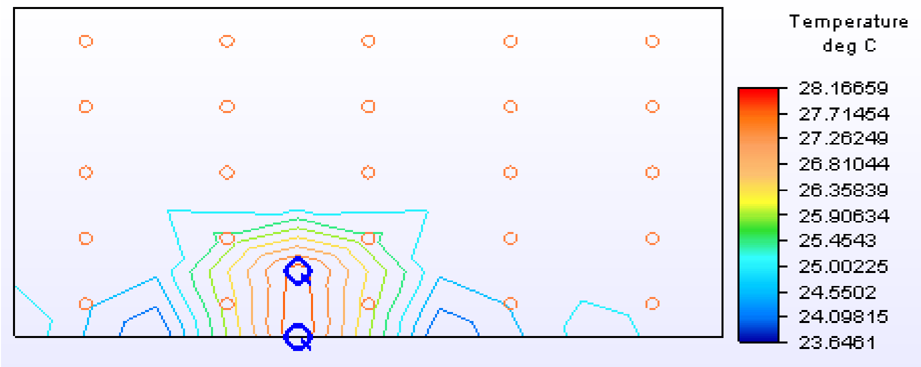

Figure 6.3: Temperature contour simulated in isolines for parameter combinations of power = 0.02 W, spatial velocity = 30 mm/min and spot size = 0.40 mm

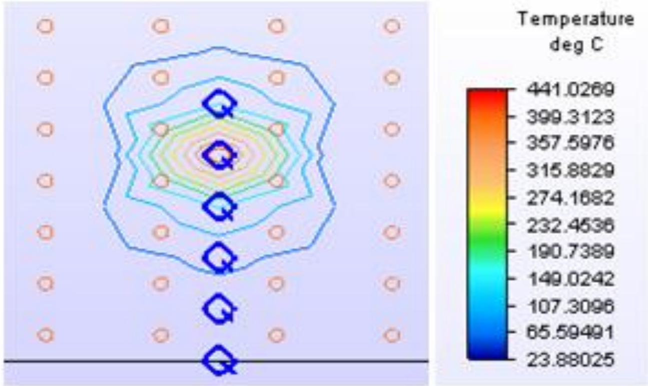

Figure 6.4: Temperature contour simulated in isolines for parameter combinations of power = 0.50 W, spatial velocity = 10 mm/min and spot size = 0.10 mm

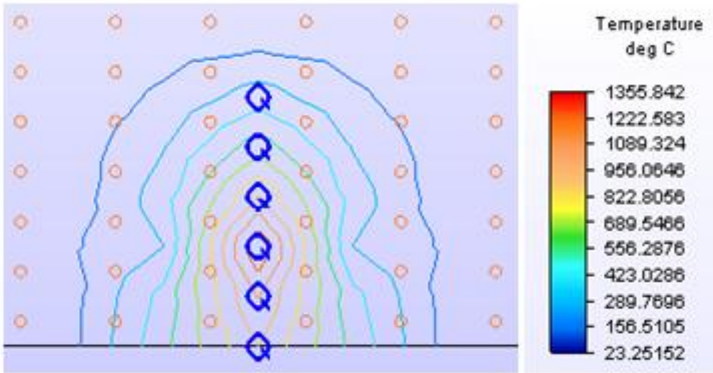

Figure 6.5: Temperature contour simulated in isolines for parameter combinations of power = 0.26 W, spatial velocity = 50 mm/min and spot size = 0.10 mm

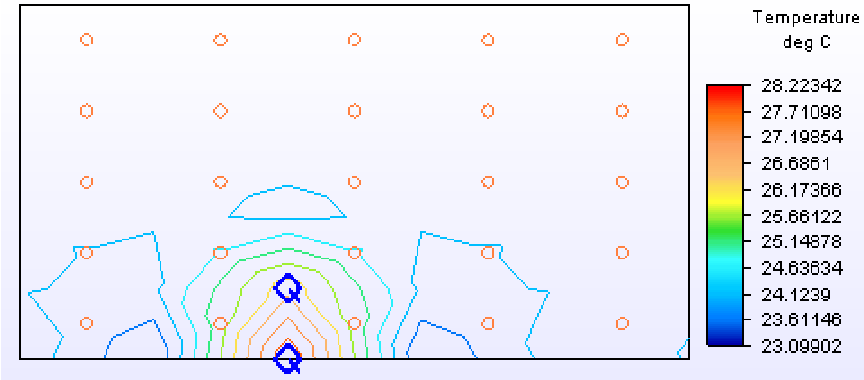

Figure 6.6: Temperature contour simulated in isolines for parameter combinations of power = 0.02 W, spatial velocity = 50 mm/min and spot size = 0.40 mm

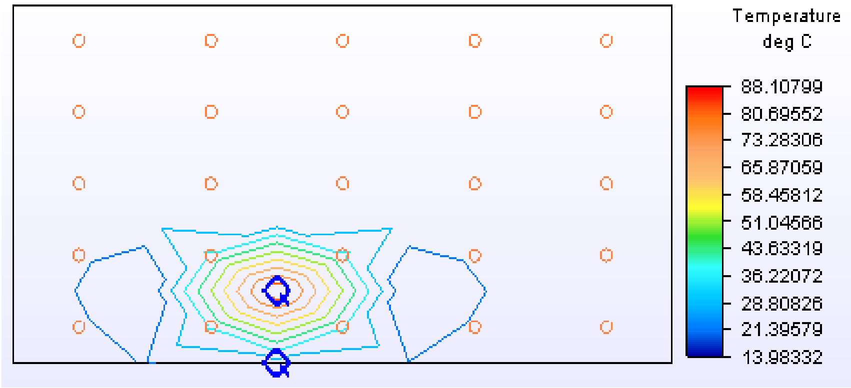

Figure 6.7: Temperature contour simulated in isolines for parameter combinations of power = 0.26 W, spatial velocity = 10 mm/min and spot size = 0.40 mm

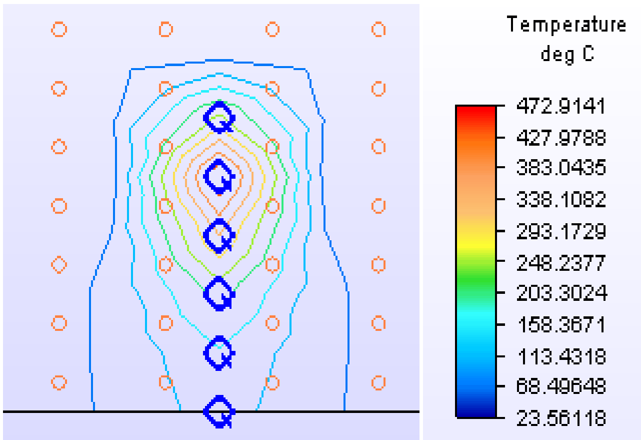

Figure 6.8: Temperature contour simulated in isolines for parameter combinations of power = 0.50 W, spatial velocity = 50 mm/min and spot size = 0.10 mm

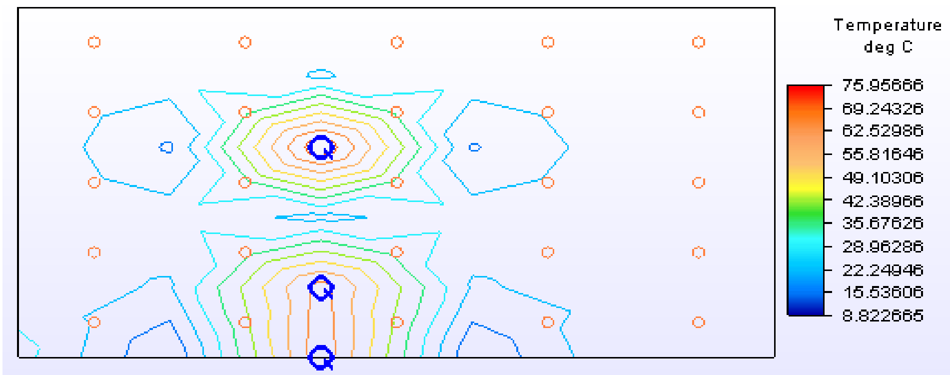

Figure 6.9: Temperature contour simulated in isolines for parameter combinations of power = 0.26 W, spatial velocity = 30 mm/min and spot size = 0.40 mm

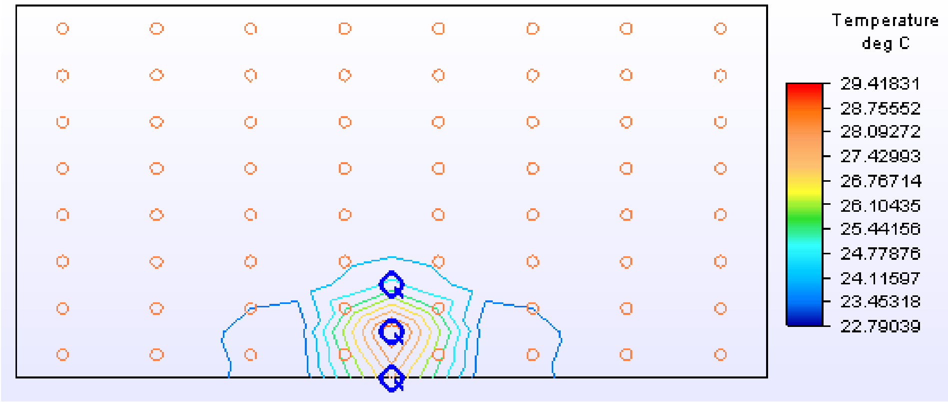

Figure 6.10: Temperature contour simulated in isolines for parameter combinations of power = 0.02 W, spatial velocity = 50 mm/min and spot size = 0.25 mm

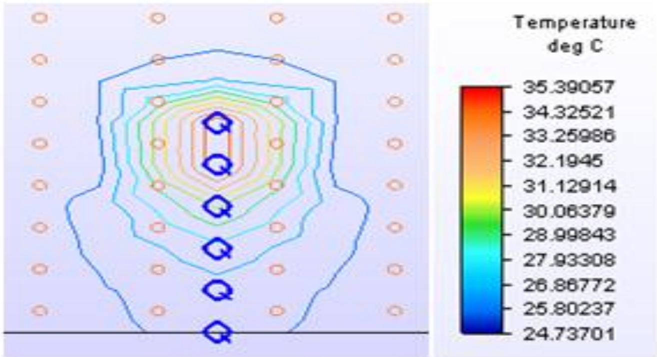

Figure 6.11: Temperature contour simulated in isolines for parameter combinations of power = 0.02 W, spatial velocity = 30 mm/min and spot size = 0.10 mm

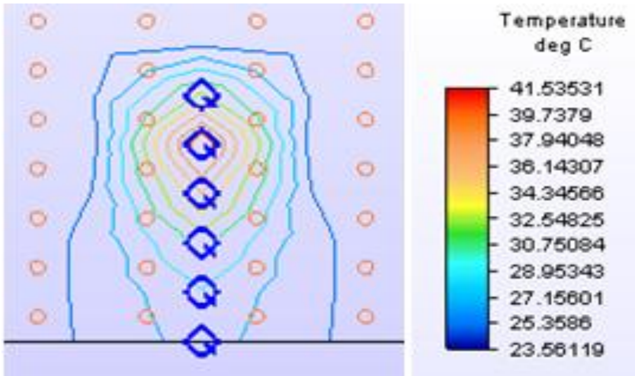

Figure 6.12: Temperature contour simulated in isolines for parameter combinations of power = 0.02 W, spatial velocity = 50 mm/min and spot size = 0.10 mm

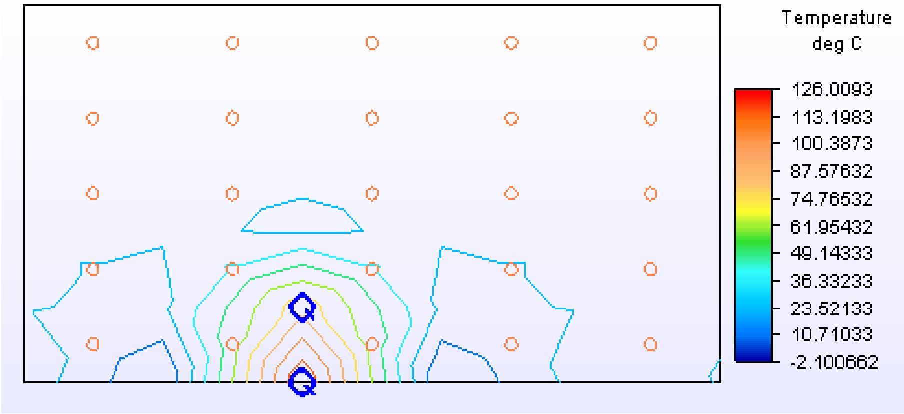

Figure 6.13: Temperature contour simulated in isolines for parameter combinations of power = 0.50 W, spatial velocity = 50 mm/min and spot size = 0.40 mm

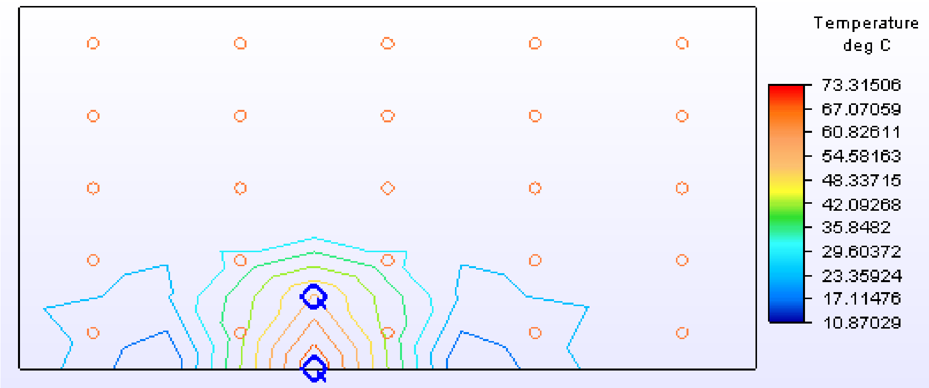

Figure 6.14: Temperature contour simulated in isolines for parameter combinations of power = 0.26 W, spatial velocity = 50 mm/min and spot size = 0.40 mm

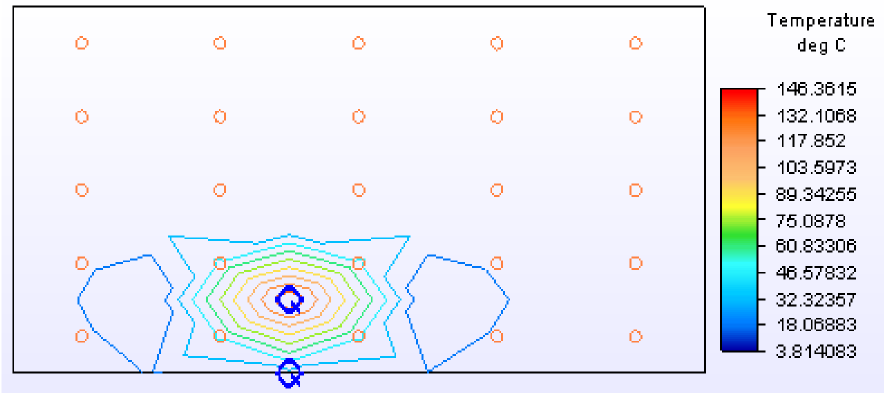

Figure 6.15: Temperature contour simulated in isolines for parameter combinations of power = 0.50 W, spatial velocity = 10 mm/min and spot size = 0.40 mm

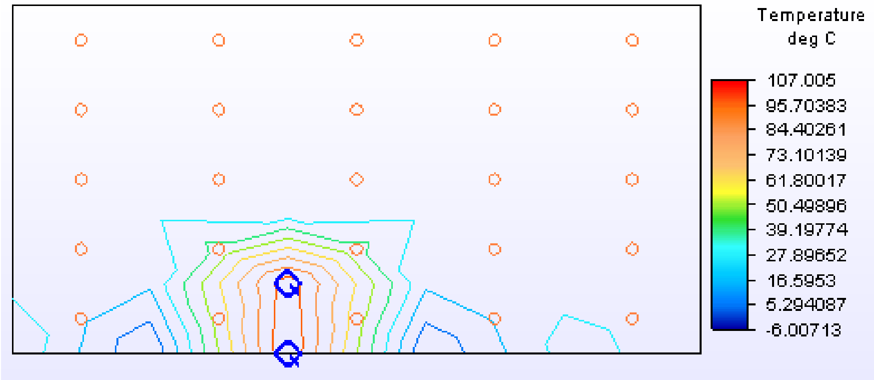

Figure 6.16: Temperature contour simulated in isolines for parameter combinations of power = 0.50 W, spatial velocity = 30 mm/min and spot size = 0.40 mm

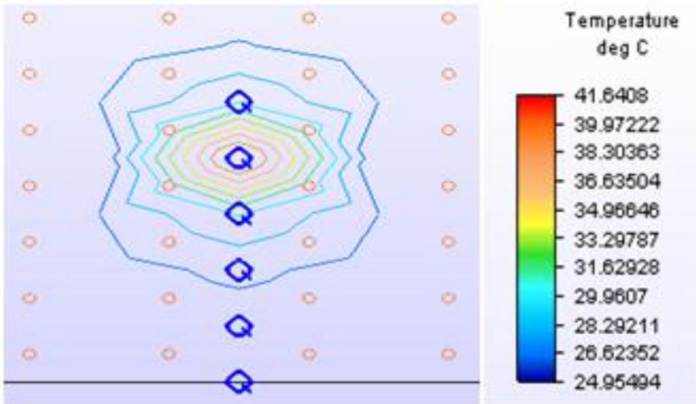

Figure 6.17: Temperature contour simulated in isolines for parameter combinations of power = 0.02 W, spatial velocity = 10 mm/min and spot size = 0.10 mm

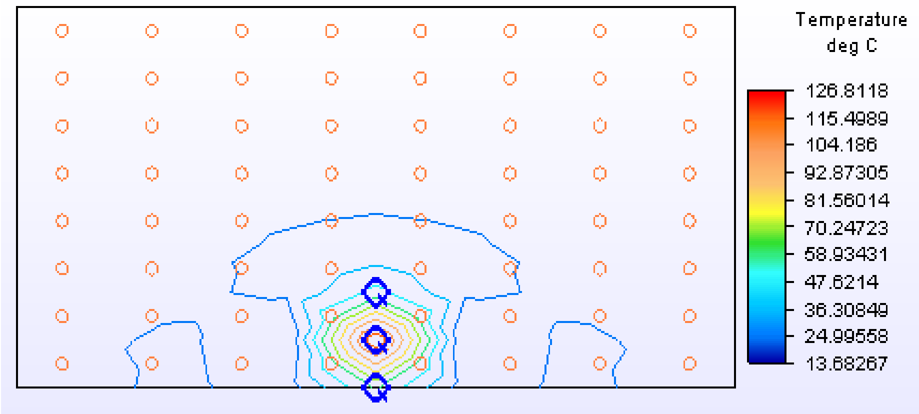

Figure 6.18: Temperature contour simulated in isolines for parameter combinations of power = 0.26 W, spatial velocity = 30 mm/min and spot size = 0.25 mm

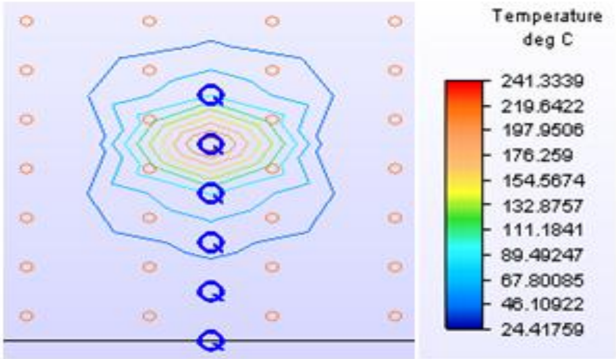

Figure 6.19: Temperature contour simulated in isolines for parameter combinations of power = 0.26 W, spatial velocity = 10 mm/min and spot size = 0.10 mm

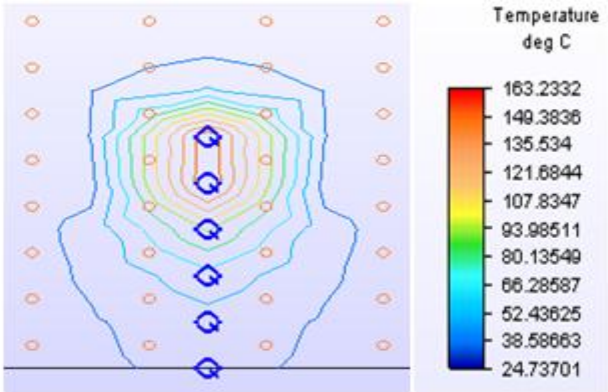

Figure 6.20: Temperature contour simulated in isolines for parameter combinations of power = 0.26 W, spatial velocity = 30 mm/min and spot size = 0.10 mm

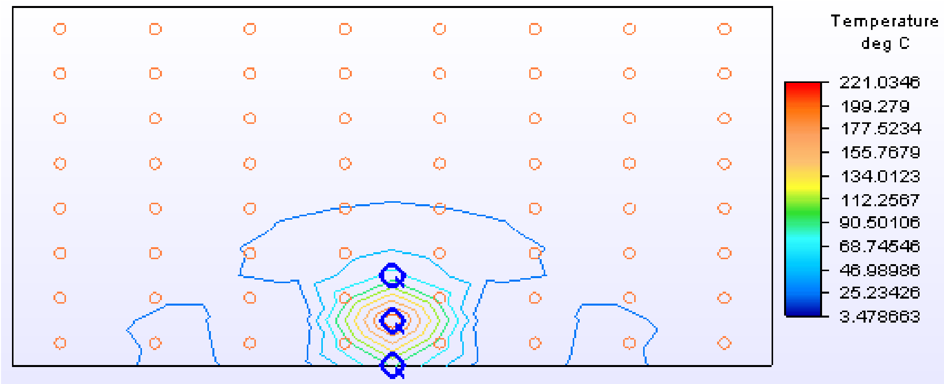

Figure 6.21: Temperature contour simulated in isolines for parameter combinations of power = 0.50 W, spatial velocity = 30 mm/min and spot size = 0.25 mm

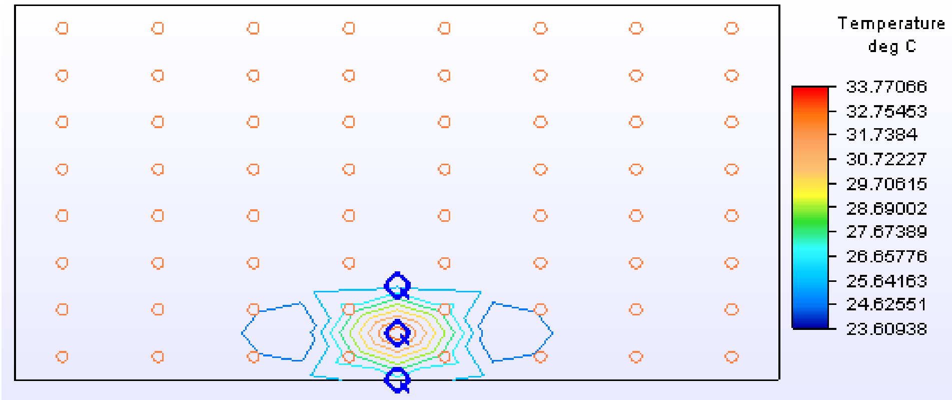

Figure 6.22: Temperature contour simulated in isolines for parameter combinations of power = 0.02 W, spatial velocity = 10 mm/min and spot size = 0.25 mm

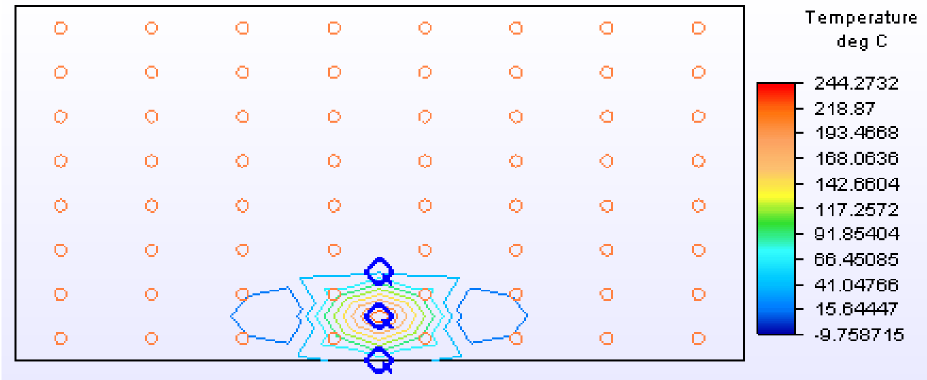

Figure 6.23: Temperature contour simulated in isolines for parameter combinations of power = 0.50 W, spatial velocity = 10 mm/min and spot size = 0.25 mm

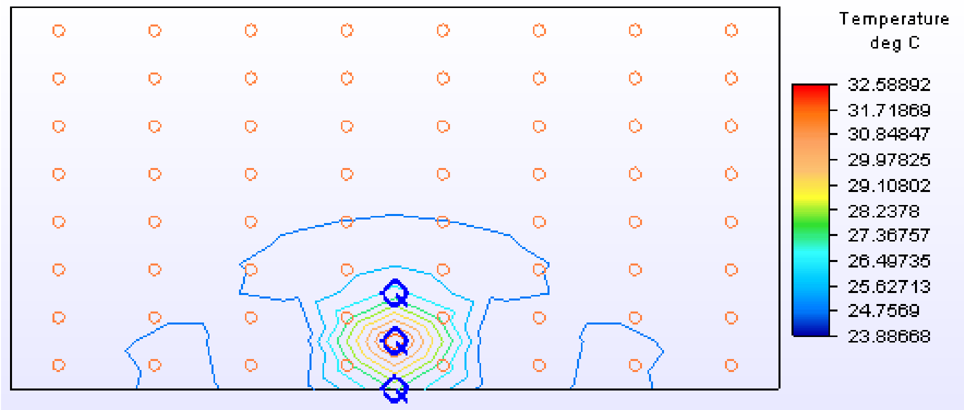

Figure 6.24: Temperature contour simulated in isolines for parameter combinations of power = 0.02 W, spatial velocity = 30 mm/min and spot size = 0.25 mm